© 2020. Published by The Company of Biologists Ltd | Journal of Cell Science (2020) 133, jcs244624. doi:10.1242/jcs.244624

RESEARCH ARTICLE

Invariant chain regulates endosomal fusion and maturation through an interaction with the SNARE Vti1b

Azzurra Margiotta[1,*], Dominik M. Frei[1,*], Ingrid Hegnes Sendstad[1], Lennert Janssen[2], Jacques Neefjes[2] and Oddmund Bakke[1,‡]

ABSTRACT

The invariant chain (Ii, also known as CD74) is a multifunctional regulator of adaptive immune responses and is responsible for sorting major histocompatibility complex class I and class II (MHCI and MHCII, respectively) molecules, as well as other Ii-associated molecules, to a specific endosomal pathway. When Ii is expressed, endosomal maturation and proteolytic degradation of proteins are delayed and, in non-antigen presenting cells, the endosomal size increases, but the molecular mechanisms underlying this are not known. We identified that a SNARE, Vti1b, is essential for regulating these Ii-induced effects. Vti1b binds to Ii and is localized at the contact sites of fusing Ii-positive endosomes. Furthermore, truncated Ii lacking the cytoplasmic tail, which is not internalized from the plasma membrane, relocates Vti1b to the plasma membrane. Knockout of Ii in an antigen-presenting cell line was found to speed up endosomal maturation, whereas silencing of Vti1b inhibits the Ii-induced maturation delay. Our results suggest that Ii, by interacting with the SNARE Vti1b in antigen-presenting cells, directs specific Ii-associated SNARE-mediated fusion in the early part of the endosomal pathway that leads to a slower endosomal maturation for efficient antigen processing and MHC antigen loading.

KEY WORDS: Endosomal fusion, Ii, Vti1b, SNAREs, MHCII

INTRODUCTION

The major histocompatibility complex class II (MHCII) molecules and the associated invariant chain (Ii, also known as CD74) are expressed in a particular set of immune cells, typically termed antigen-presenting cells (APCs). In addition, the MHCII and Ii molecules may be induced in non-APCs by IFNγ and other stimuli (Neefjes et al., 2011). MHCII is expressed as heterodimers composed of two non-covalently associated type I (N-terminal in the lumen) transmembrane polypeptides. These highly polymorphic molecules bind to short polypeptides derived from endocytosed protein antigens and present these to the T-cell receptors on $CD4^+$ T-cell clones. Ii is a non-polymorphic type II transmembrane protein that forms complexes by self-trimerization in the endoplasmic reticulum (ER) and that provides a scaffold for the assembly of three MHCII heterodimers. The rate of synthesis of Ii is significantly higher than that of MHCII (Machamer and Cresswell, 1982), and in general there is more Ii protein than MHCII in antigen-presenting cells, although Ii has a short half-life of a few hours, and the half-life of MHCII is 1–2 days (Kampgen et al., 1991; Landsverk et al., 2012; Schroder, 2016). Ii then sorts several other associated molecules, including the neonatal Fc receptor (also known as FCGRT) (Ye et al., 2008) and major histocompatibility complex class I (MHCI; Basha et al., 2012; Walchli et al., 2014) to the endosomal pathway (reviewed in Schroder, 2016).

Importantly, Ii, which contains two efficient leucine-based endosomal sorting signals, facilitates the exit of MHCII from the ER in antigen-presenting cells and mediates rapid transport of the MHCII–Ii complex, via the plasma membrane (PM), to the endosomal pathway where the MHCII receptor is loaded with antigen (Bremnes et al., 1994; Bakke and Dobberstein, 1990; Elliott et al., 1994; Bikoff et al., 1993; Neefjes and Ploegh, 1992; McCormick et al., 2005; Dugast et al., 2005; Wang et al., 1997; Liu et al., 1998; Brachet et al., 1999; Sevilla et al., 2001; Caplan et al., 2000). In addition, Ii delays transport of endosomal content from Rab5-positive early endosomes (EE) to late Rab7a-positive endosomes (LE) (Gorvel et al., 1995). Ii also induces fusion of early endosomes creating enlarged endosomes (Pieters et al., 1993; Romagnoli et al., 1993). Ii-positive endosomes are able to mature normally, but with a prolonged residence time in EE (indicated by the presence of EEA1 and Rab5) before the endosomes switch to late, acidic Rab7a- and Lamp1-positive multivesicular endosomes and lysosomes (Stang and Bakke, 1997; Landsverk et al., 2011). Such a delayed endosomal pathway is found to improve MHCII antigen presentation (Gregers et al., 2003).

Most membrane fusion events in the cell require SNARE (soluble N-ethylmaleimide-sensitive factor attachment protein receptor) proteins (reviewed in Jahn and Scheller, 2006). All SNAREs share the conserved SNARE motif of 60–70 amino acids (Weimbs et al., 1997) and often contain a transmembrane domain. However, some SNAREs are anchored to membranes by lipid modifications. There are several types of SNARE domains; R-SNAREs contribute an arginine residue to the binding layer of the assembled complex, whereas Q-SNAREs have conserved glutamine residues (Fasshauer et al., 1998). Q-SNAREs are further subdivided into Qa-, Qb- and Qc-SNAREs depending on their position in the complex. One SNARE domain of each class is required to form the complex. The formation of this complex provides the driving power necessary for membrane fusion.

Homotypic fusion of early endosomes can be blocked by phosphatidylinositol 3-kinase (PI3K) inhibitors (Jones and Clague, 1995; Powis et al., 1994). Notably, this is not the case for homotypic fusion of Ii-positive endosomes *in vivo* and *in vitro* (Nordeng et al., 2002). This indicates that the Ii-associated fusion mechanisms differ from the standard early endosomal fusion

[1]Department of Molecular Biosciences, University of Oslo, PB 1066, 0316 Oslo, Norway. [2]Department of Cell and Chemical Biology, Oncode Institute, Leiden University Medical Center LUMC, Leiden, The Netherlands.

*These authors contributed equally to this work

‡Author for correspondence (oddmund.bakke@ibv.uio.no)

A.M., 0000-0002-0639-4931; L.J., 0000-0001-9705-0204; J.N., 0000-0001-6763-2211; O.B., 0000-0003-4843-7626

Handling Editor: David Stephens
Received 27 January 2020; Accepted 25 August 2020

Journal of Cell Science (2020) 133, jcs244624. doi:10.1242/jcs.244624

machinery. However, the Ii-induced fusion of endosomes can be inhibited by N-ethylmaleimide (NEM), suggesting that SNARE molecules are involved in this process. So far, it is not known which SNARE proteins drive Ii-mediated endosome fusion. Here, we show that the Q-SNARE Vti1b is a key regulator of Ii-induced endosome fusion. Vti1b depletion reduced Ii-induced endosomal size, indicating a functional role in this process. This was further substantiated by a co-isolation of Vti1b with Ii. Vti1b was found enriched at contact sites between Ii-positive endosomes and was present at the fusion pore. As a further proof, depletion of Vti1b abrogated the effect of Ii-induced delay in endosomal maturation. These data suggest that Vti1b is an essential element in an Ii-mediated delayed endosomal pathway.

RESULTS

Ii regulates endosomal maturation in antigen-presenting cells

Intracellular trafficking studies showing that Ii induces a delayed endosomal maturation are based on non-APCs transfected with Ii and MHCII (Gorvel et al., 1995; Landsverk et al., 2011). To see whether this effect could also be seen in APCs, we used the well-known human cell line MelJuSo, which endogenously expresses the MHCII, invariant chain and associated molecules, although they are not professional antigen-presenting cells (Pieters et al., 1991; Paul et al., 2011; Bayer-Santos et al., 2016). Ii is well expressed in these cells, and we generated Ii-knockout (Ii KO) cells using CRISPR-Cas9 to test for the influence of Ii on endosomal maturation. The absence of Ii in the Ii KO cells was verified by western blotting (Fig. S4B). The progression from early endosomes to late endosomes in MelJuSo wild-type cells (wt; expressing Cas9 enzyme) and Ii KO cells was studied using live-cell imaging. We followed single endosomes until the exchange from an mApple–Rab5 to an EGFP–Rab7 coat (Landsverk et al., 2011). As seen in Fig. 1, the time until the exchange from Rab5 to Rab7 coat on single endosomes was significantly shorter in Ii KO MelJuSo cells compared to the time taken in wt control cells. Rab5-positive endosomes in the control cells acquired the Rab7 coat after 23 min, whereas this exchange was seen after 11 min in Ii KO cells (Fig. 1B). This suggests that Ii regulates endosomal maturation not only in model fibroblast-like cell lines transfected with Ii, but also in cells expressing basically all components of professional MHCII antigen-presenting cells.

To test whether knockout of Ii influenced the size or the number of early endosomes in the MelJuSo cells, we measured these parameters using immunofluorescence (Fig. 1C–G). We labelled early compartments in control and Ii KO cells using EEA1 as a marker (Fig. 1C). Although the average size of early endosomes was not affected by Ii (Fig. 1D,E), the subset of endosomes larger than 1 µm was significantly reduced in the absence of Ii (Fig. 1F), in line with data showing that Ii increases the endosomal size when expressed in cell lines (Pieters et al., 1993; Romagnoli et al., 1993). However, the number of endosomes larger than 1 µm in the MelJuSo cells represented, only a small subset of early endosomes, and we detected no significant change in the total number of early endosomes in Ii KO cells compared to the number in control cells (Fig. 1G), and we cannot conclude that this is physiologically relevant.

Vti1b is involved in Ii-mediated endosome enlargement

When Ii is expressed in non-antigen-presenting cells, the size of the endosomal compartments increases (Pieters et al., 1993; Romagnoli et al., 1993). In fact, there is a positive correlation between the size increase and Ii-expression levels (Nordeng et al., 2002). It has been shown that both the Ii-induced delayed endosomal maturation and the induced enlargement of endosomes are dependent on Ii trimerization and the presence of a net negative charge in the Ii cytoplasmic tail, suggesting that these two effects might be caused by similar mechanisms (Nordeng et al., 2002; Gregers et al., 2003; Landsverk et al., 2009).

We have found previously that NEM, a chemical compound that blocks, amongst others, SNARE proteins, can inhibit Ii-driven endosomal fusion (Nordeng et al., 2002), and this led us to test for the contribution of SNAREs. To test for SNAREs involved in Ii-mediated endosome enlargement, we used the M1 fibroblast cell line stably transfected with Ii under the control of a heavy-metal-inducible promoter (M1 pMep4-Ii; Nordeng et al., 2002). The M1 wild-type cell line is negative for Ii and the MHCII proteins, and the cell line has been employed extensively to study endosomal dynamics and antigen presentation by transfection with immune genes (Roche et al., 1993; Stang and Bakke, 1997; Skjeldal et al., 2012; Sand et al., 2014; Haugen et al., 2017; Long et al., 1994).

Ii transport to Ii-positive endosomes was here visualized by adding fluorescently tagged antibody recognizing the extracellular/luminal domain of Ii, and the size of Ii-positive endosomes was analysed by confocal microscopy. First, we employed some of the known inhibitors of early endosome fusion (Fig. 2A). The MAP kinase inhibitor SB203580 (Cuenda et al., 1995) was used to block Rab5 activation, and wortmannin was used to inhibit PI3K activity (Wymann et al., 1996). In agreement with earlier reports (Nordeng et al., 2002), neither wortmannin nor SB203580 affected the endosomal enlargement induced by Ii (Fig. 2A). This indicates that MAP kinase and PI3K activity are non-essential for the Ii-induced endosomal enlargement. However, NEM, a general inhibitor of SNARE function, significantly reduced Ii-mediated endosome enlargement by ∼50% (Fig. 2A).

We thereafter evaluated the endosomal size of Ii-positive endosomes when single human SNAREs were depleted using RNAi. The M1 pMep4-Ii cells were transfected with control siRNA or siRNA targeting the SNARE and were subsequently treated with $CdCl_2$ to induce Ii expression. Interestingly, we found that silencing of Vti1b could abrogate the Ii-induced endosome enlargement, whereas Vti1b had no effect when the active mutant of Rab5 (Rab5Q79L) (Stenmark et al., 1994; Wegner et al., 2010) was expressed in order to increase endosome size (Fig. 2D–F). Western blot analyses confirmed that the two different siRNAs against *VTI1B* efficiently reduced level of the Vti1b target protein (Fig. 2B,C). We also quantified the number of endosomes per cell in the above experiment and observed that the silencing of Vti1b significantly increased the number of endosomes after Ii expression, indicating that silencing of Vti1b inhibits the Ii-mediated increased endosomal size (Fig. 2G,H). On the other hand, silencing of Vti1b had no effect on the number of endosomes when the endosomes were enlarged as a result of expression of Rab5Q79L (Fig. 2G,H), suggesting that the Vti1b effect is not a general requirement for enlarging early endosomes, but is more specific for the Ii-induced endosomal enlargement.

As a control we also silenced Vti1B in M1 cells where no Ii was expressed, but found no change in size and number of endosomes (Fig. S1A–D). The average size of EEA1-positive endosomes was ∼0.8 µm diameter, both in control cells and in VTI1B-depleted cells (Fig. S1B,C). In order to confirm the role of Ii in enlarging early endosomes, we transfected mCherry–Ii, together with its untagged version (needed for the mCherry–Ii to egress the ER), in M1 cells and stained for EEA1, showing that the diameter of the endosomes could increase several folds upon Ii expression (Fig. S1E).

Journal of Cell Science (2020) 133, jcs244624. doi:10.1242/jcs.244624

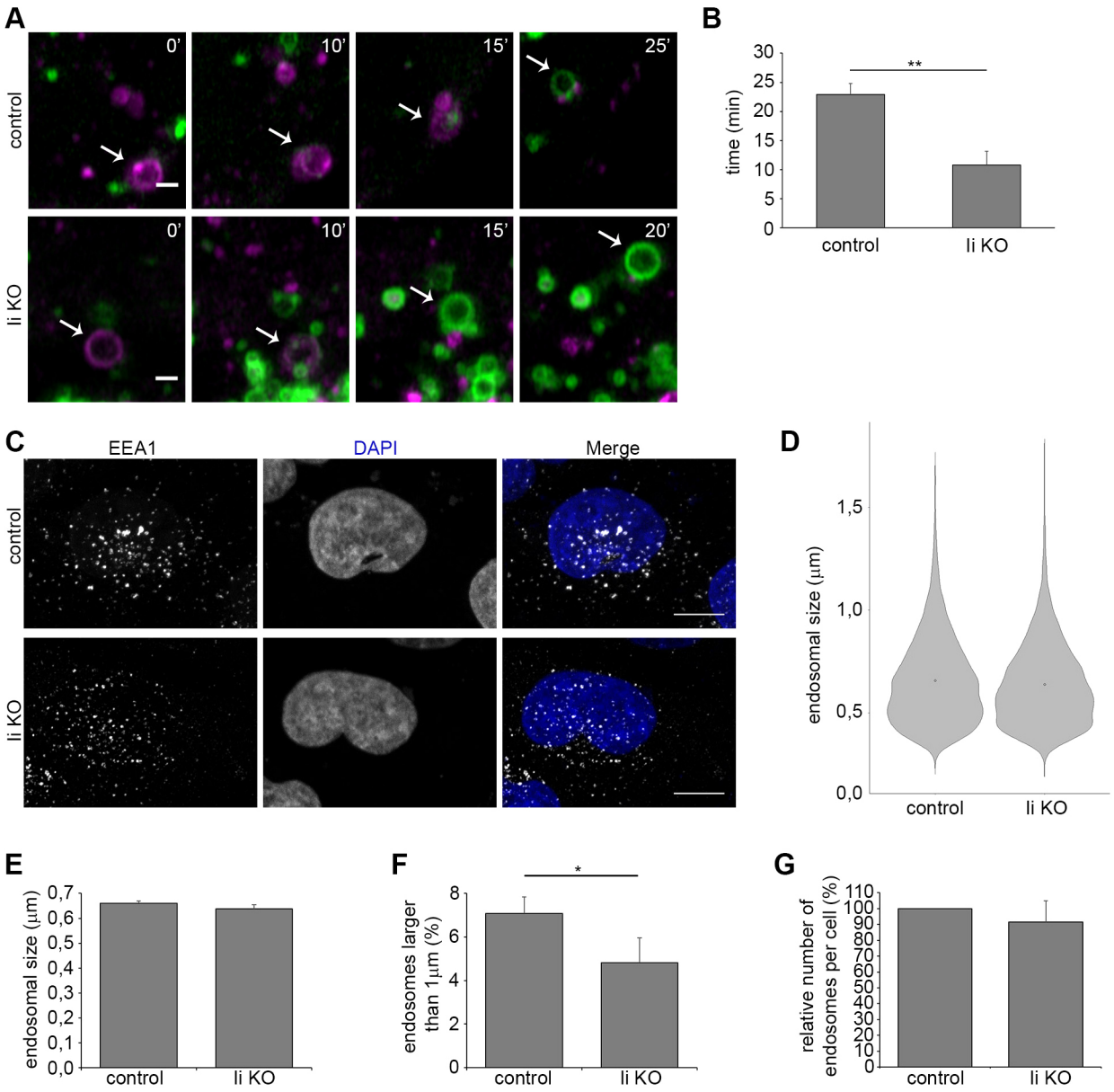

Fig. 1. Ii knockout speeds up maturation in APCs. (A) MelJuSo control or Ii KO cells were transfected with mApple–Rab5 (magenta) and EGFP–Rab7 (green). Single endosomes were followed over time (frame interval 30 s). Time after start of observation in minutes is indicated in each image. Arrows indicate an endosome that undergoes Rab5 to Rab7 transition. Scale bar: 1 µm. (B) Quantification of the time until the Rab5–Rab7 switch in MelJuSo cells expressing Cas9 (control) or Ii knockout (Ii KO) is shown. Mean±s.e.m. for three independent experiments. The bars represent average value of multiple endosomes (41 for control, 53 for Ii KO cells) from several cells. (C) MelJuSo control and Ii KO cells seeded on coverslips were permeabilized, fixed and labelled using anti-EEA1 antibodies (grey) and DAPI (nuclei, blue). Scale bar: 10 µm. (D) The distribution of the size of EEA1-positive endosomes in control and Ii KO MelJuSo cells is shown in the violin plot (more than 2900 endosomes per sample in total were analysed). (E) Average size of EEA1-positive endosomes in control and Ii KO cells (more than 32 cells in total per sample were analysed). Mean±s.e.m. of three independent experiments. (F) Quantification of the percentage of EEA1-positive endosomes larger than 1 µm in control and Ii KO MelJuSo cells. More than 2900 endosomes were analyzed for each sample. (G) Quantification of the relative number of EEA1-positive endosomes in control and Ii KO cells. More than 32 cells were analysed per sample. *P<0.05; **P<0.01 (two-tailed Student's t-test).

Vti1b localized to docking sites between Ii-positive endosomes during their fusion

Given the well-documented role of SNARE proteins in membrane fusion, we decided to study the localization of Vti1b in M1 pMep4-Ii cells transfected with Ii and Vti1b–mCitrine. Interestingly, cells expressing Vti1b–mCitrine showed that this SNARE protein is localized at the contact sites between Ii-positive endosomes (Fig. 3A,B). When the endosomes were small (up to 1.5 µm) (Fig. 3A), generally we saw one domain of Vti1b, whereas for larger endosomes (Fig. 3B) more Vti1b domains were observed. The Vti1b–mCitrine domains were usually found at the contact sites between two Ii-positive endosomes (Fig. 3C top row), and quantification showed that Vti1b accumulated at ∼80% of the contact sites between Ii-positive endosomes (Fig. 3D). We conducted the same instead using mCherry–Rab5Q79L to induce enlarged endosomes (Fig. 3C bottom row). Vti1b also clustered at the contact zone between Rab5Q79L-positive endosomes, but this was only seen for 40% of the endosomal contact sites. This shows that Vti1b has a significant preference to be present at the contact site of

Journal of Cell Science (2020) 133, jcs244624. doi:10.1242/jcs.244624

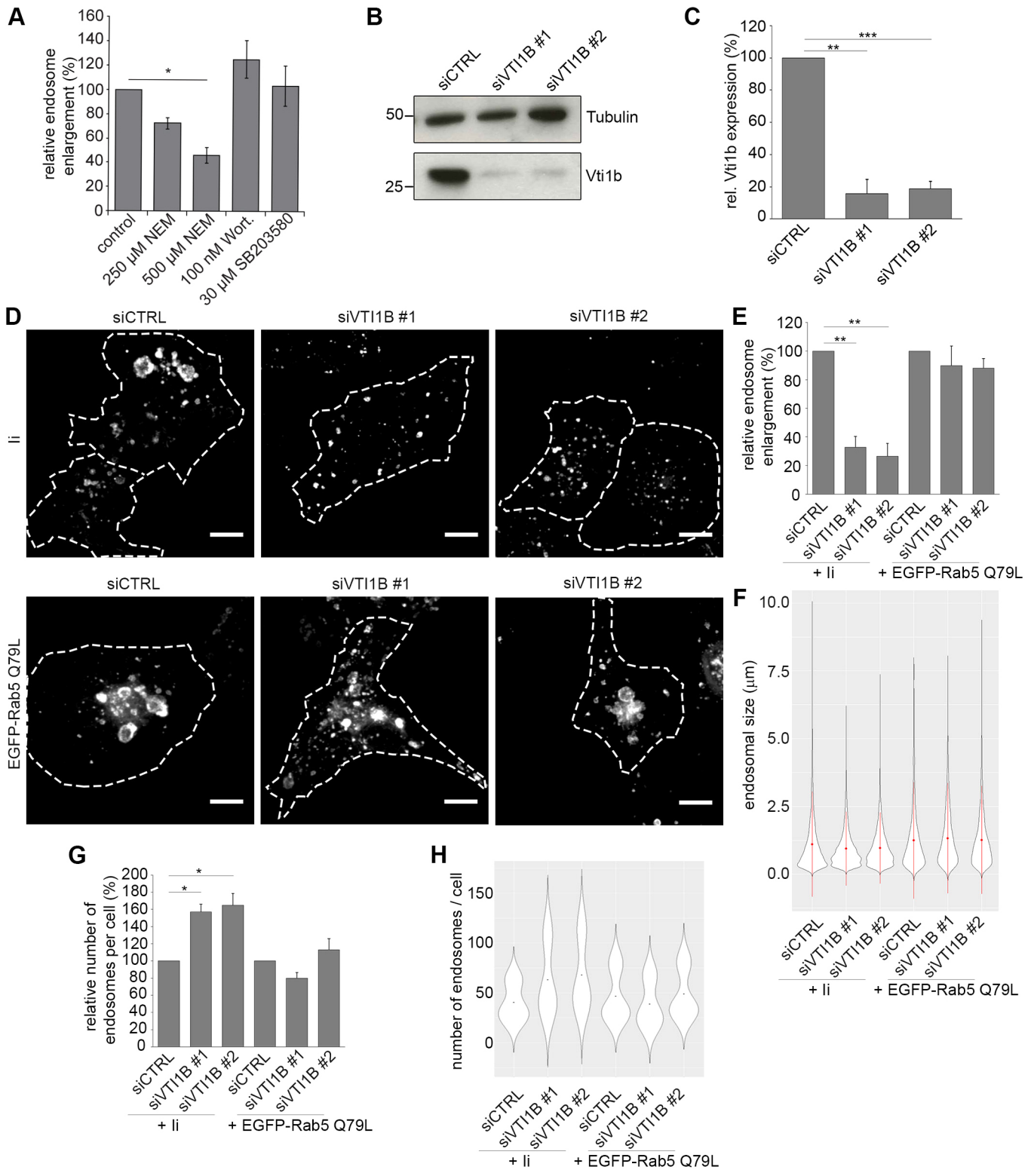

Fig. 2. See next page for legend.

fusing Ii-positive endosomes, as compared to contact sites in Rab5Q79L-induced enlarged endosomes. We also observed that Vti1b–mCitrine localized to contact sites between Ii-positive endosomes in MelJuSo cells (Fig. 3E), indicating that Vti1b also associated with invariant chain at endosomal contact sites in antigen-presenting cells.

Vti1b interacts with Ii

Because Vti1b has a role in the regulation of the Ii-mediated endosomal enlargement and colocalizes with Ii, we tested whether this SNARE could interact with Ii. First, we transfected either EGFP (as a negative control) or Vti1b–mCitrine into M1 pMep4-Ii cells. The expression of Ii was induced by overnight $CdCl_2$ treatment, and

Journal of Cell Science (2020) 133, jcs244624. doi:10.1242/jcs.244624

Fig. 2. Ii-induced enlargement of endosomes is dependent on Vti1b. (A) Results of endosome quantification after treatment of M1 pMep4-Ii cells with different drugs affecting early endosome fusion, mean±s.e.m. of three independent experiments. Wort., wortmannin. (B) M1-pMep4-Ii cells transfected with control siRNA (siCTRL) or siRNAs against Vti1b (siVTI1B #1 and siVTI1B #2) were lysed and subjected to western blot analysis using anti-Vti1b and anti-tubulin antibodies. Detection of tubulin was used as loading control. (C) Quantification of Vti1b abundance is shown. Data represent the mean±s.e.m. of three independent experiments. (D) M1-pMep4-Ii cells were transfected with control siRNA or siRNAs targeting VTI1B. After 48 h of transfection, cells were either treated overnight with 7 µM $CdCl_2$ to induce Ii expression (top row) or transfected with EGFP–Rab5Q79L (bottom row). Cells expressing Ii were treated with anti-Ii antibody coupled with an Alexa Fluor 488 fluorescent dye for 30 min before fixation and imaging. Confocal images are shown. Dashed lines indicate the shape of the cells. Scale bars: 10 µm. (E) Quantification of the percentage of endosomes (diameter ≥3 µm) in control and Vti1b-silenced cells expressing either Ii or EGFP–Rab5Q79L. Data represent the mean±s.e.m. of three different experiments (n=50). (F) Violin plot showing the distribution of endosome size (Feret's diameter) in the various conditions. Red dot and line indicate mean±s.d. Number of endosomes analysed per condition was >1600. (G) Quantification of the number of endosomes per cell in control and Vti1b-silenced cells expressing either Ii or Rab5Q79L. Data represent the mean±s.e.m. of three different experiments. (H) Violin plot showing the distribution of endosome number per cell in the various conditions. Black dot indicates the mean. Number of cells per condition analysed >60. *P<0.05; **P<0.01; ***P<0.001 (two-tailed Student's t-test).

we then performed a co-immunoprecipitation (co-IP) experiment using anti-GFP nanobodies (which also recognize mCitrine). We evaluated the presence of Ii in the eluates by western blotting (Fig. 4A). We observed a band indicating the presence of Ii after immunoprecipitation of Vti1b–mCitrine with anti-GFP antibodies but not for the control EGFP (Fig. 4A), showing that Vti1b interacts with Ii. In order to further elucidate the interaction between Vti1b and Ii, we transfected Vti1b–mCitrine and full-length wild-type His-tagged Ii (His–Ii wt) or Ii lacking the cytoplasmic tail (His–Δ27Ii) in HeLa cells. As a negative control, we used cells co-transfected with EGFP and His–Ii wt. Then, we performed a co-IP assay using anti-GFP nanobodies (Fig. 4B). Interestingly, Vti1b–mCitrine interacted with full-length Ii and with His–Δ27Ii (Fig. 4B), showing that the cytoplasmic tail of Ii is dispensable for binding to Vti1b.

Invariant chain lacking the cytoplasmic tail relocates Vti1b to the plasma membrane

Vti1b contains a very short luminal domain (three amino acids) and a long cytoplasmic tail (Brunger, 2005), whereas Ii has a short (30 amino acids) cytoplasmic domain and a long luminal domain (Koch et al., 1989). Ii without a cytoplasmic tail is known to localize to the PM (Bakke and Dobberstein, 1990). To characterize the localization of these two associated proteins, we co-expressed Ii lacking the cytoplasmic tail, tagged with a hexahistidine tag (His–Δ27Ii), and Vti1b–mCitrine in HeLa cells and, as control, the same set up using full-length Ii. Vti1B with full-length Ii localized to intracellular vesicles including, Ii-positive endosomes, similar to the localization in Vti1B-transfected cells without Ii (Fig. 5). However, when Vti1B was co-expressed with His–Δ27Ii, a large fraction of Vti1b colocalized with His–Δ27Ii at the PM, and less Vti1b was localized to vesicles, as quantified in Fig. 5B. Because Vti1b was found to bind to both Ii wild-type Ii and His–Δ27Ii, and part of the Vti1b was relocated to the PM by His–Δ27Ii, this suggests that these two molecules are associated in the biosynthetic pathway and that Vti1b could be guided by Ii to the endosomal pathway when Ii is expressed.

The influence of Ii knockout on Vti1b distribution in antigen-presenting cells

In the intracellular trafficking experiments above, we transfected wild-type or mutant Ii into cells lacking MHCII and associated genes (i.e. M1 and Hela cells), and it was of interest to see whether lack of Ii could influence the distribution of Vti1b in MelJuSo cells, which endogenously express genes in a similar manner to APCs (Paul et al., 2011). To test for this, we transfected Vti1b–mCitrine into MelJuSo Ii KO and MelJuSo control cells followed by fixation and labelling with anti-CI-M6PR, an antibody that labels the trans-Golgi network (TGN) and endosomes (Fig. 6). Interestingly, Vti1b–mCitrine colocalized more with CI-M6PR (also known as IGF2R) in the Ii KO cells as compared with colocalization in the control cells (Fig. 6A,B). We also evaluated the number of vesicles positive for Vti1b–mCitrine, which was drastically reduced to about 40 vesicles/cell in the Ii KO cells, as compared to an average of 240 vesicles/cell for control cells (Fig. 6C). The volume of the CI-M6PR-positive structures in the Ii KO and control MelJuSo cells was not significantly different (Fig. 6D). As shown in Fig. 6, we were able to rescue the phenotype by transfecting cDNA for Ii into the Ii KO cells. This indicates that the altered intracellular distribution of Vti1b is indeed caused by the Ii KO and not by an off-target effect. Interestingly, these vesicles positive for Vti1b and Ii were also Rab5- or Rab7-positive (Fig. S2). In fact, we transfected Vti1b–mCitrine in MelJuSo control cells together with either mcherry–Rab5 or mApple–Rab7 and stained for endogenous Ii. Approximately 80% of endosomes positive for both Vti1b and Ii were also Rab7-positive, whereas 20% of the Vti1b- and Ii-positive endosomes were Rab5-positive, indicating that Vti1b and Ii are found in both early and late endosomes (Fig. S2).

CI-M6PR localizes in the trans-Golgi, the plasma membrane and the late endosomal pathway (Hille-Rehfeld, 1995). To better establish the localization of Vti1b in the MelJuSo Ii KO cells, we also analysed the colocalization of Vti1b with the Golgi-resident protein giantin (also known as GOLGB1; Linstedt and Hauri, 1993) and with TGN46 (also known as TGOLN2), which mainly resides in the TGN (Prescott et al., 1997). As shown in Fig. 7, more colocalization with both of these Golgi proteins was observed in the Ii KO cells.

Vti1b has been reported to be in a complex with other endosomal SNARE proteins (Antonin et al., 2000; Wade et al., 2001; Pryor et al., 2004). However, the colocalization of CI-M6PR with fusion proteins of Vamp7, Stx8 and Vamp8 was not altered in the Ii KO cells (Fig. S3), indicating that the effect of Ii is not general for endosomal SNAREs and is possibly specific for Vti1b.

Vti1b is expressed in APCs and its protein levels are not affected by Ii expression

Given the important role of Ii in professional APCs and in antigen presentation (reviewed in Schroder, 2016), we determined Vti1b protein level in APCs and other cell types. The expression levels of Vti1b in monocyte-derived dendritic cells (DCs), EBV-immortalized B cells, the melanoma cell line MelJuSo, HeLa, Raji, M1 and Neuro2A cells were analysed by western blotting (Fig. S4A). Vti1b was widely expressed (Fig. S4A). To test whether Ii affects the expression levels of this SNARE protein, we analysed the melanoma cell line MelJuSo (Fig. S4B,C), assaying both control and Ii KO cells. The expression of Vti1b was not affected by Ii expression. Similarly, high levels of Ii expression in M1 pMep4-Ii cells after induction with $CdCl_2$ (Fig. S4D) also did not affect Vti1b expression (Fig. S4E). Ii expression does not affect endogenous Vti1b expression.

Journal of Cell Science (2020) 133, jcs244624. doi:10.1242/jcs.244624

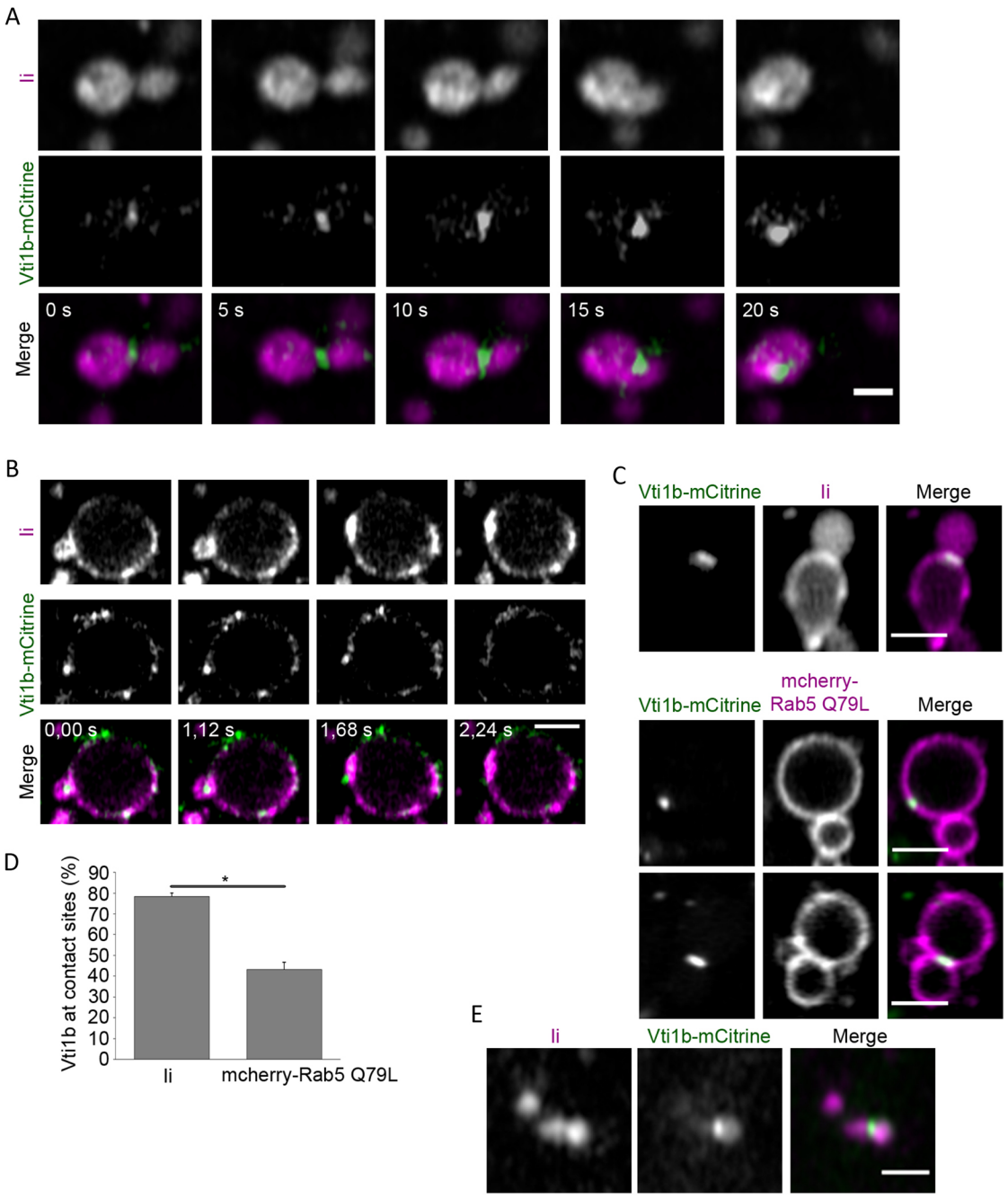

Fig. 3. Vti1b localizes to contact sites at Ii-positive endosomes during fusion. (A,B) M1 pMep4-Ii cells were transiently transfected with Vti1b–mCitrine overnight, and Ii was expressed for 8 h (7 µM $CdCl_2$ treatment). Cells were treated with anti-Ii antibody coupled with Alexa Fluor 555 for 1 h before live-cell imaging. Time-lapse confocal images of Ii (magenta) and Vti1b–mCitrine (green) during endosome fusion are shown. Scale bar: 1 µm in A, 2 µm in B. (C) M1 pMep4-Ii cells were either transiently transfected with Vti1b–mCitrine (green) and treated with 7 µM $CdCl_2$ for 8 h to induce Ii expression (top, magenta) or co-transfected with Vti1b–mCitrine and mCherry–Rab5Q79L (bottom, magenta). Cells expressing Ii were treated with anti-Ii antibody coupled with an Alexa Fluor 647 fluorescent dye antibody for 1 h before live imaging using Fast AiryScan. Two images from cells transfected with mCherry–Rab5Q79L are shown, representing the somewhat different localization of Vti1b in different cells. Scale bars: 2 µm. (D) Quantification of the percentage of transfected Vti1b localized at the contact sites in cells expressing Ii or mCherry–Rab5Q79L is shown. Data represent the mean±s.e.m. of three independent experiments. (E) MelJuSo cells transfected with Vti1b–mCitrine were labeled with anti-Ii antibody coupled to Alexa Fluor 647 for 4 h before fixation. Representative images of endosomes positive for Ii (magenta) and Vti1b–mCitrine (green) are shown. Scale bar: 1 µm. *P<0.05 (two-tailed Student's t-test).

Silencing of Vti1b abrogates the endosomal maturation delay induced by Ii

Ii expression delays endosomal maturation from early Rab5-positive endosomes to late Rab7-positive endosomes (Gorvel et al., 1995; Landsverk et al., 2011), which correlates with Ii-induced endosomal enlargement (Nordeng et al., 2002; Gregers et al., 2003). From this, one may predict that depletion of Vti1b also counteracts the Ii-induced endosomal maturation delay, and we tested this hypothesis next.

The rate of endosomal maturation was determined by measuring the extent of colocalization of the fluorescent fluid-phase marker dextran–Alexa Fluor 488 with Lysotracker Deep Red, as a function

Journal of Cell Science (2020) 133, jcs244624. doi:10.1242/jcs.244624

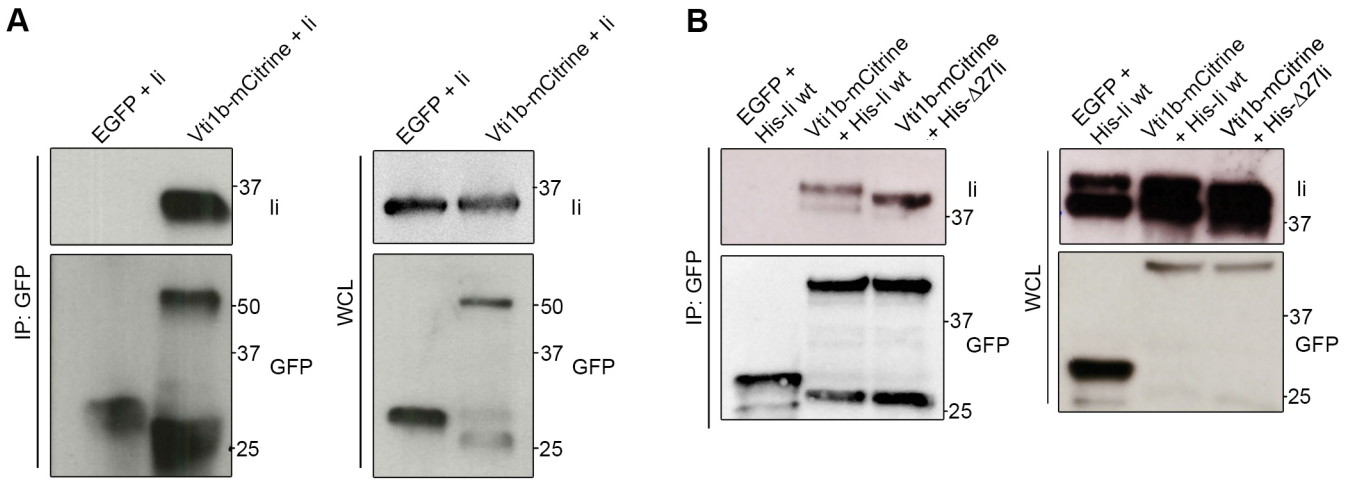

Fig. 4. Vti1b interacts with Ii. (A) M1-pMep4-Ii wild-type cells were transiently transfected with EGFP or Vti1b–mCitrine, and Ii expression was induced by treatment with $CdCl_2$ overnight. Cells were lysed and co-IP was performed using GFP-Trap magnetic beads. Whole-cell lysates (WCL, right) and immunoprecipitated samples (IP, left) were subjected to western blot analysis. (B) HeLa cells were transiently co-transfected with either EGFP or Vti1b–mCitrine and His-tagged wild-type or mutated Ii (His–Ii wt and His–Δ27Ii, respectively), as indicated in the figure. Cells were lysed after 24 h of transfection and thereafter co-IP with GFP-Trap magnetic beads was performed. Whole-cell lysates and immunoprecipitates were subjected to western blot analysis. GFP and Ii were visualized using the corresponding anti-GFP or anti-Ii antibodies. Images shown are representative of three experiments.

of time in live cells. When we performed the assay in M1 pMep4-Ii cells without inducing Ii, 52% of dextran localized with Lysotracker Deep Red after 35 min. When expression of Ii was induced using $CdCl_2$, the colocalization of dextran with Lysotracker was strongly delayed, with only 20% overlap after 35 min (Fig. 8A). This again was dependent on Vti1b, because silencing of Vti1b before induction of Ii expression abrogated the Ii-mediated delayed maturation, and the rate of endosomal maturation was similar to that in uninduced cells. Moreover, we checked whether the effects that we observed were due to different internalization rates of dextran. However, this was not the case, because the number of dextran-positive vesicles at the initial time point was similar in all samples (Fig. 8B). This suggests that Vti1b is essential for the Ii-induced delay in endosomal maturation.

Because Vti1b depletion was able to abrogate Ii-induced delay in endosomal maturation in M1 cells, we next tested its role in the MelJuSo wild-type and Ii KO cells. When we treated the wild-type cells with siRNAs targeting *VTI1B* and transfected them with mApple–Rab5 and EGFP–Rab7, we observed that the time until the exchange from Rab5 to Rab7 coat on single endosomes was 20 min for control cells (Fig. 8C,D), whereas depletion of Vti1b decreased the time required for the Rab5 coat to be exchanged with a Rab7 coat. The Rab5-positive endosomes in the Vti1b-silenced cells acquired the Rab7 coat after 15 (for *VTI1B* siRNA #1) or 12 (for *VTI1B* siRNA #2) minutes, similar to our earlier data in MelJuSo Ii KO cells. These results in antigen-presenting cells corroborate the data from the M1 cells, showing that Vti1b is required by Ii for inducing the delay in endosomal maturation. To test whether this effect was specific for cells with Ii, we also depleted *VTI1B* in Ii KO cells and found that, in this case the Rab5–Rab7 coat exchange was not affected (Fig. S5), supporting the conclusion that the role of Vti1b in endosomal maturation is via interaction with Ii.

DISCUSSION

Invariant chain associates with MHCII, and the first function to be described for the protein was an ability to sort MHCII molecules to intracellular endosomal compartments. It was later shown that Ii actively sorts other molecules to the endosomal pathway, such as CD1 and MHCI, both molecules that participate in antigen presentation to specific T cells (for reviews see Neefjes et al., 2011; Schroder, 2016). Another striking feature of Ii is its ability to delay endosomal maturation in non-antigen-presenting cells (Gorvel et al., 1995; Landsverk et al., 2011). In addition, Ii has ‘fusogenic’ properties, because Ii expression in cells leads to homotypic fusion of early endosomes (Nordeng et al., 2002; Romagnoli et al., 1993; Stang and Bakke, 1997). This had led to the hypothesis that Ii is a key immunological molecule that is essential for creating a subset of endosomes called ‘immunoendosomes’ suitable for slowly processing endosomal contents for optimal antigen loading (Neefjes et al., 2011). The MHCII-positive multivesicular late endosomal compartment in antigen-presenting cells (Peters et al., 1991) should therefore be a typical immunoendosome. The idea that Ii may delay endosomal maturation was, until now, only based on observations of fibroblast cells transfected with Ii (Gorvel et al., 1995), which may differ from antigen-presenting cells. Here we show that Ii KO in the antigen-presenting MelJuSo cells also affects endosomal maturation, in this case resulting in faster maturation (Fig. 1A,B). A correlation has been found between the Ii-induced enlarged early endosomes and Ii-induced maturation delay, and mutations of the charged residues from negative to positive in the cytoplasmic tail of Ii abrogate both effects (Gregers et al., 2003; Nordeng et al., 2002) indicating that similar mechanisms are involved in both.

How could Ii regulate the endosomal pathway? An NMR study has shown that the cytoplasmic tails of Ii could interact in trans and possibly interact in homotypic fusion (Motta et al., 1997). Ii has a short cytoplasmic tail of 30 amino acids, which would prevent it from acting as a genuine SNARE. It is thus more likely that other molecules are recruited to Ii to assist in regulating the endosomal pathway. We have also showed previously that EEA1 and Rab5 are not essential for the Ii-induced fusion and enlargement of endosomes (Nordeng et al., 2002). However, the chemical compound NEM, which inhibits the SNARE function, blocks fusion and formation of Ii-induced enlarged endosomes (Nordeng et al., 2002), bringing our attention to the involvement of SNAREs in this the process.

Journal of Cell Science (2020) 133, jcs244624. doi:10.1242/jcs.244624

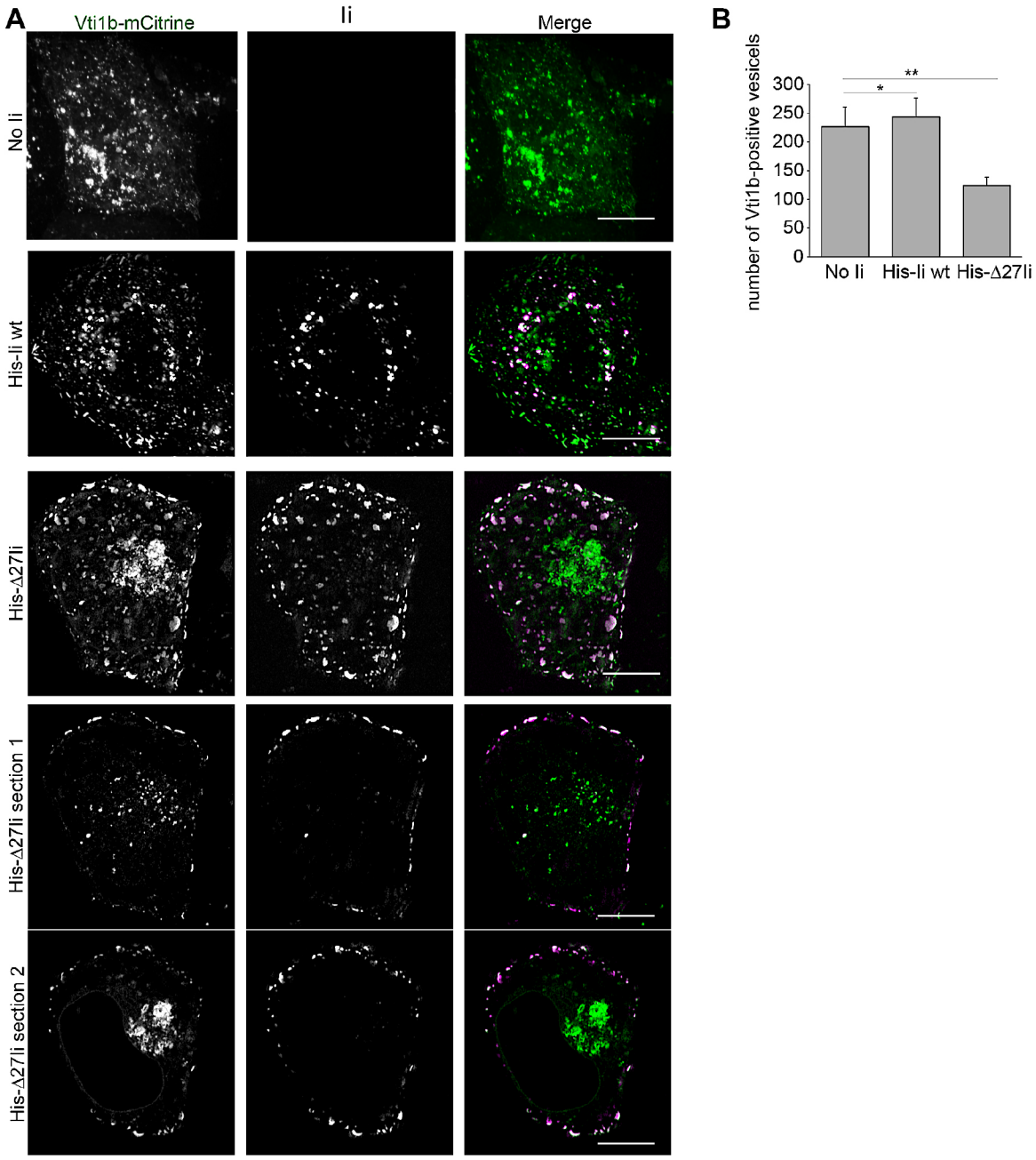

Fig. 5. Vti1b and His–Δ27Ii colocalize at the plasma membrane. (A) HeLa cells were transfected with Vti1b–mCitrine alone (No Ii) or co-transfected together with His-tagged wild-type or mutated Ii (His–Ii wt and His–Δ27Ii, respectively), as indicated in the figure. Confocal images are shown. Upper three rows represent maximum intensity projections. Given the complex localization of Vti1b when His–Δ27Ii was expressed, the bottom two rows represent arbitrary single focal planes of the cell transfected with Vti1b–mCitrine and His–Δ27Ii in order to show: in section 1, the vesicular and PM localization; and in section 2, perinuclear distribution of Vti1b–mCitrine. Scale bars: 10 µm. (B) Quantification of the number of Vti1b–mCitrine-positive vesicles in HeLa cells transfected as indicated. Data represent the mean±s.e.m. of at least two independent experiments. At least 11 cells per condition were analysed. *P<0.05; **P<0.01 (two-tailed Student's t-test).

By screening a SNARE siRNA library, we observed that silencing of the Qb SNARE Vti1b strongly decreased Ii-induced endosomal size changes (Fig. 2B–H). Interestingly, although Vti1b has a major role in the fusion of late endosomes, it has not been implicated in the fusion of early endosomes (Luzio et al., 2009; Pryor et al., 2004; Kreykenbohm et al., 2002; Antonin et al., 2000). Taken together, this suggests that Ii employs a SNARE complex that is independent of the canonical early endosomal fusion machinery. This seems to be specific for Ii, because we found that enlargement of endosomes induced by the expression of the constitutively active mutant of Rab5, Rab5Q79L (Wegner et al., 2010) was not affected by Vti1b silencing (Fig. 2D–H). Interestingly, the reduction of the size of Ii-positive endosomes was accompanied by an increase in the number of Ii-positive endosomes, corroborating that Ii-induced enlargement of endosomes is due to an increase in endosomal fusion between Ii-positive endosomes, rather than reduced fission.

In support of these data, we demonstrated that transfected Vti1b was preferentially localized at the contact sites of Ii-positive endosomes (Fig. 3). Strikingly, the effect was highly pronounced for the Ii-enlarged endosomes, and Vti1b was detected at 80% of

Journal of Cell Science (2020) 133, jcs244624. doi:10.1242/jcs.244624

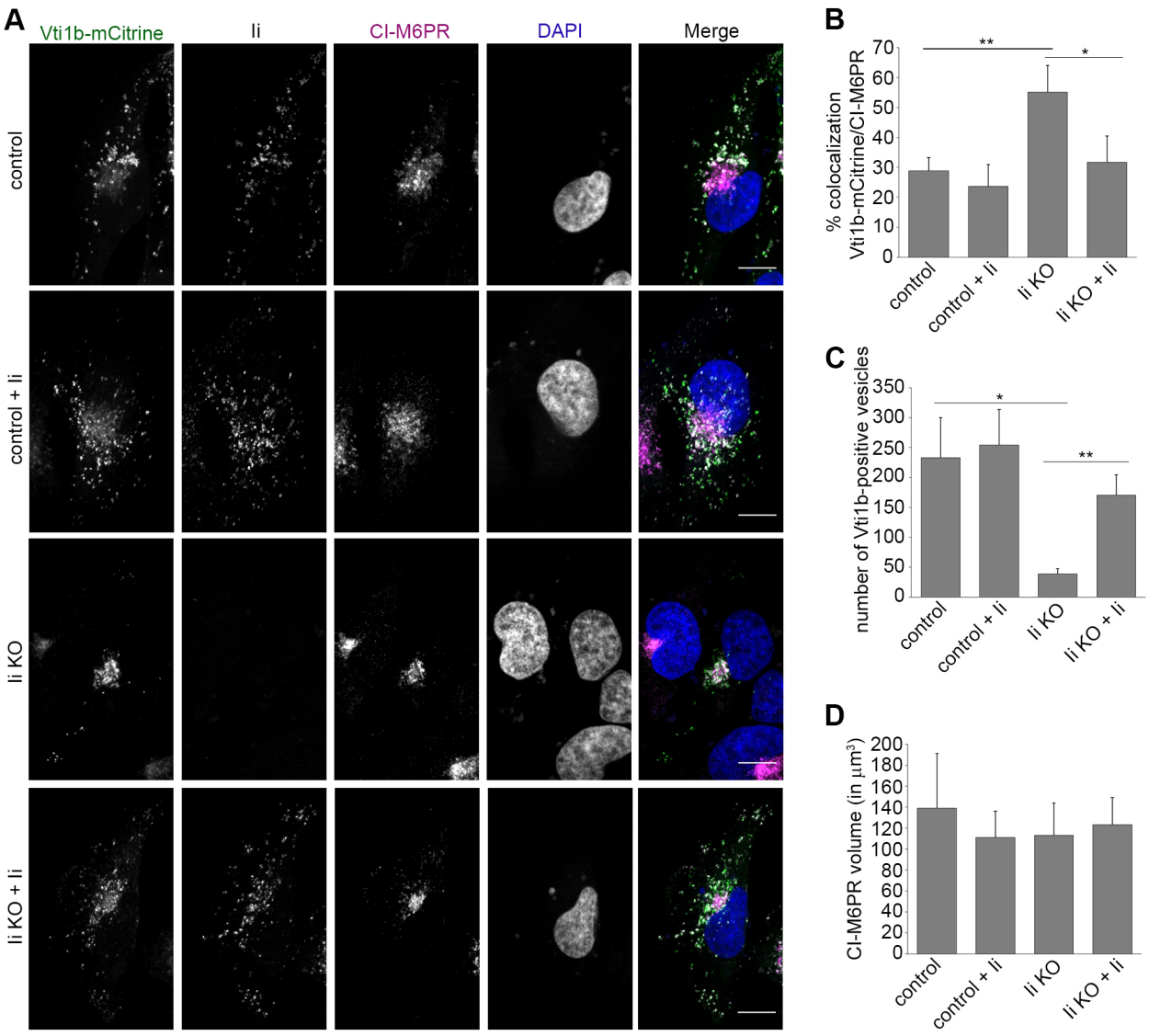

Fig. 6. Vti1b localization is altered in MelJuSo Ii KO cells. (A) MelJuSo control and Ii KO cells transfected with Vti1b–mCitrine were either transfected with His–Ii (+Ii) or not, as indicated in the figure, and subsequently labelled live for Ii by treating the cells with an anti-Ii antibody coupled with Alexa Fluor 647 for 4 h. Cells were stained after fixation with an anti-CI-M6PR antibody and DAPI. Representative images (maximal projections) of Vti1b–mCitrine (green), Ii (grey), CI-M6PR (magenta) and nuclei (blue, DAPI), and a merge image, are shown. Scale bars: 10 µm. (B) Quantification of the percentage of colocalization between Vti1b–mCitrine and CI-M6PR in control, Ii-overexpressing (control+Ii), Ii KO or Ii-transfected Ii KO cells (Ii KO+Ii) is shown. (C) Quantification of the number of vesicles per cell positive for Vti1b–mCitrine in control, Ii-overexpressing, Ii KO or Ii-transfected Ii KO cells. (D) Quantification of the volume of CI-M6PR positive structure in the indicated samples. Data represent the mean±s.e.m. of at least three independent experiments. At least 50 cells per condition were analysed. *P<0.05; **P<0.01 (two-tailed Student's t-test).

the endosome–endosome contact points. Using expression of Rab5Q79L to enlarge endosomes, we found that Vti1b was only seen in 40% of the contact sites. This indicates that Vti1b is located at the fusion domain of the endosome and that invariant chain expression positively influences the location of Vti1b at this site. Immunoprecipitation studies showed that Vti1b binds to Ii, directly or indirectly, and this interaction may be the reason for the presence of Vti1b in the contact zone between Ii-positive endosomes (Fig. 4). The fact that His-tagged Ii lacking the cytoplasmic tail (His–Δ27Ii) also co-immunoprecipitated Vti1b suggests that the interaction is indirect or via the transmembrane domains of the two proteins.

When M1 cells were not transfected with any Ii expression construct, Vti1b was located mainly on endosomes. However, when Ii lacking the cytoplasmic tail (His–Δ27Ii) was expressed, a large fraction of Vti1b was retained at the PM, together with His–Δ27Ii. This confirms that this mutated version of Ii is able to interact with Vti1b. When wild-type Ii was expressed, Vti1b relocated to the endosomal pathway, indicating that the Vti1b-bound fraction is sorted by wild-type Ii. Taken together, this supports a model where Vti1b is sorted to endosomes in non-antigen-presenting cells without Ii, whereas Ii is able to dominate the sorting of a fraction of Vti1b when this molecule is expressed in APCs.

We also noticed that the distribution of Vti1b was shifted to the perinuclear region and that there were correspondingly fewer Vti1b-positive vesicles when Ii was deleted in the Ii KO MelJuSo cells (Figs 6, 7). This suggests that in MelJuSo cells, Vti1b has adapted to endosomal sorting with Ii, and when Ii is removed this causes a shift in the localization of Vti1b, that is, less Vti1b is sorted to the endosomal pathway.

Journal of Cell Science (2020) 133, jcs244624. doi:10.1242/jcs.244624

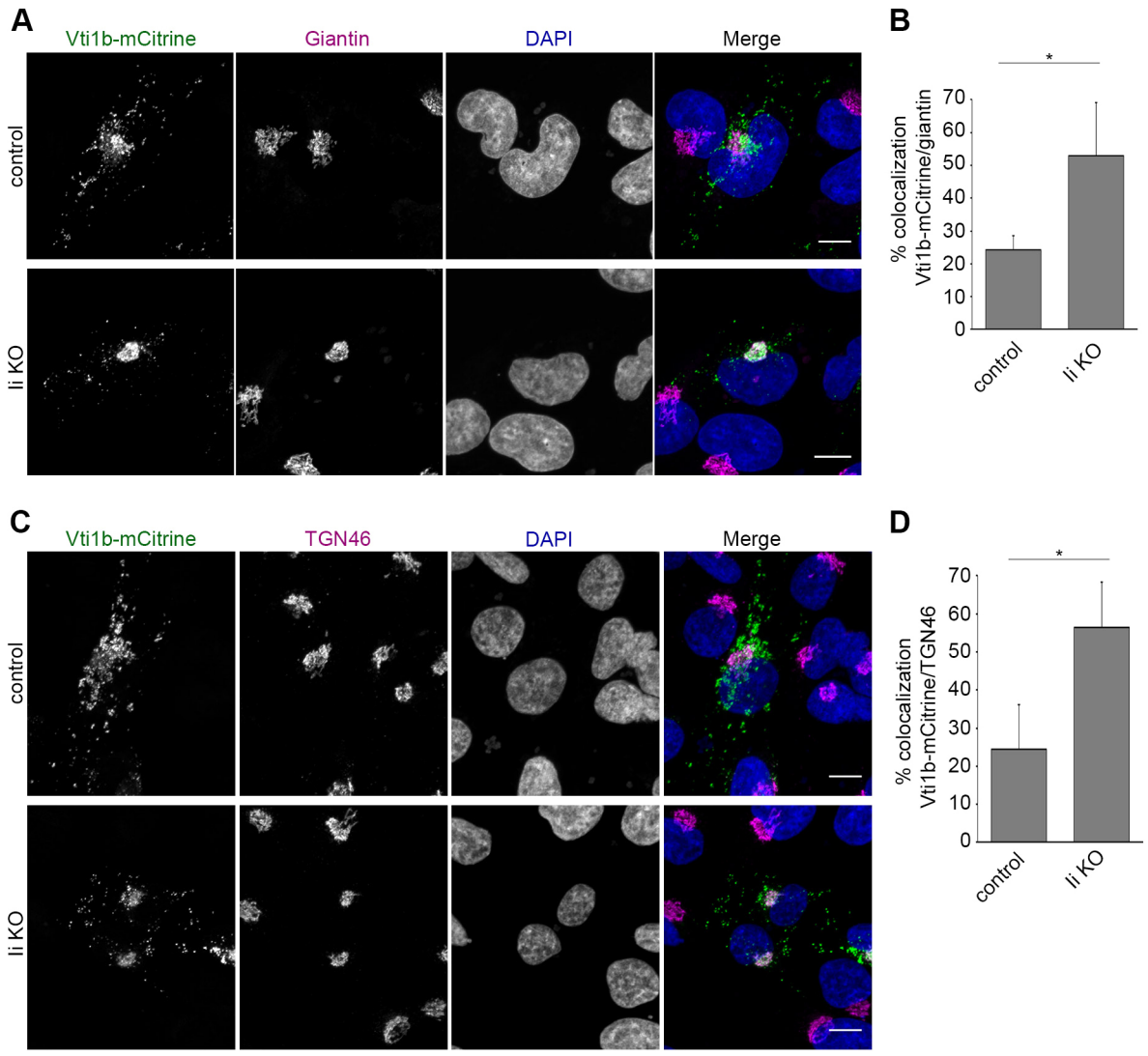

Fig. 7. Vti1b shows increased localization to giantin- and TGN46-positive structures in MelJuSo Ii KO cells. (A) MelJuSo control and Ii KO cells were transfected with Vti1b–mCitrine and subsequently stained after fixation with an anti-giantin antibody and DAPI. Representative images (maximal projections) of Vti1b–mCitrine (green), giantin (magenta) and nuclei (blue, DAPI), and a merge image, are shown. Scale bars: 10 µm. (B) Quantification of the percentage of colocalization between Vti1b–mCitrine and giantin in control and Ii KO cells is shown. (C) MelJuSo control and Ii KO cells were transfected with Vti1b–mCitrine and subsequently stained after fixation and permeabilization with an anti-TGN46 antibody and DAPI. Representative images (maximal projections) of Vti1b–mCitrine (green), TGN46 (magenta) and nuclei (blue, DAPI), and a merge image, are shown. Scale bars: 10 µm. (B) Quantification of the percentage of colocalization between Vti1b–mCitrine and TGN46 in control and Ii KO cells is shown. At least 50 cells per condition were analysed. Data represent the mean±s.e.m. **P*<0.05 (two-tailed Student's *t*-test).

Vti1b, as well as its yeast homologue Vti1p, is a versatile molecule that can be in different complexes and adopt different localization depending on its regulation (Antonin et al., 2000; Von Mollard et al., 1997; Fischer von Mollard and Stevens, 1999). Vti1b has also been implicated in several different trafficking pathways where it participates in regulating fusion and/or maturation (Antonin et al., 2000; Pryor et al., 2004; Nozawa et al., 2017; Furuta et al., 2010; Offenhauser et al., 2011). Furthermore, Vti1b is reported to be part of a SNARE complex that functions in the fusion of LEs (Antonin et al., 2000). Indeed, Vti1b is important for homotypic fusion of LEs, whereas only a weak effect of Vti1b was detected on homotypic fusion of EEs when using the SNARE antibody to inhibit endosomal fusion *in vitro* (Antonin et al., 2000). In addition, another SNARE complex containing Vti1b is able to regulate the heterotypic fusion between LEs and lysosomes (Pryor et al., 2004).

In immune cells, Vti1b plays an important role in different trafficking pathways that are of relevance for the immune response (Dressel et al., 2010; Manderson et al., 2007; Murray et al., 2005). In macrophages, it regulates both the exocytic and endocytic pathways by taking part in different SNARE complexes (Murray et al., 2005; Manderson et al., 2007; Offenhauser et al., 2011) and it is fundamental for the trafficking of proinflammatory cytokines from the TGN to recycling endosomes (Manderson et al., 2007; Murray et al., 2005). In cytotoxic T-lymphocytes (CTLs), killing capacity is mainly mediated by exocytosis of cytotoxic proteins in lytic granules, specialized secretory lysosomes, and this is dependent on Vti1b (Dressel et al., 2010; Qu et al., 2011). Moreover, Vti1b is found on recycling endosomes that transport newly synthetized perforin, independently of lytic granules, from the TGN to the PM (Lesteberg et al., 2017).

Journal of Cell Science (2020) 133, jcs244624. doi:10.1242/jcs.244624

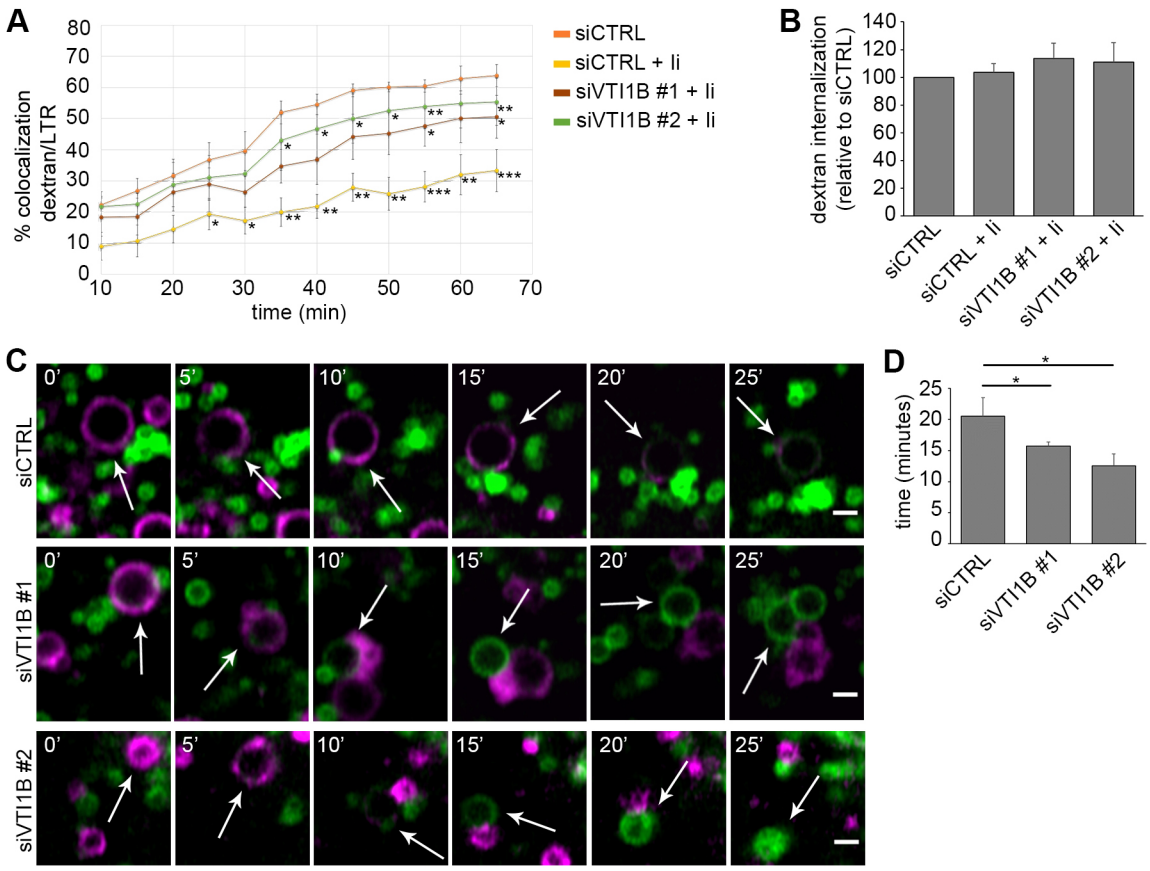

Fig. 8. Ii causes a delay in trafficking dependent on Vti1b. (A) Colocalization of dextran and Lysotracker Deep Red (LTR) in M1 pMep4-Ii cells expressing Ii (+Ii), or not, and treated with control siRNA (siCTRL) or siRNAs against *VTI1B* (siVTI1B #1 and siVTI1B #2), as indicated. Data represent the mean±s.e.m. of at least three independent experiments. **P*<0.05; ***P*<0.01; ****P*<0.001 (one-way repeated measures ANOVA followed by Tukey's post hoc test). (B) Quantification of the number of dextran-positive vesicles at the start of the imaging. More than 40 cells per condition were analysed. Data are mean±s.e.m. (C) MelJuSo control cells treated with control RNA or individual VTI1B siRNAs were transfected with mApple–Rab5 (magenta) and GFP–Rab7 (green). Single endosomes were followed over time (frame interval 30 s). Time after start of observation in minutes is indicated in each image. Arrows indicate typical single endosomes that undergo transition from Rab5 (magenta) to Rab7 (green). Scale bars: 1 µm. (D) Quantification of the time until the Rab5–Rab7 switch is shown. Mean±s.e.m. for at least three independent experiments. The data are presented as mean±s.e.m. of multiple endosomes (55 for control RNA, 71 for VTI1B siRNA #1, 47 for VTI1B siRNA #2 cells) from several cells. The measurements of each individual endosome depend on its visibility in time and space and, as such, is not precisely accurate. **P*<0.05 (two-tailed Student's *t*-test).

Furthermore, Vti1b functions are regulated by another SNARE protein, syntaxin11 (Stx11), which is highly expressed in cells of the immune system. Stx11 binds Vti1b, possibly with other regulatory proteins, and modulates its availability in different SNARE complexes, thus regulating the trafficking steps between late endosomes, lysosomes and the cell surface in macrophages (Offenhauser et al., 2011). Intriguingly, expression of Stx11 is able to affect Vti1b complex formation with sets of Q-SNARE partners, whereas its depletion causes enlargement of LEs, an increased trafficking from LEs to the PM and a reduced fusion of LEs with lysosomes (Offenhauser et al., 2011).

Similarly to Stx11, Ii binds Vti1b and regulates its availability on different compartments and endosomal fusion and maturation. Therefore, we could speculate that Ii might have a regulatory role on Vti1b in APCs, similar to that of Stx11 in macrophages. Moreover, Vti1b can move from TGN to late endosomes by binding to the AP1 interactor Clint1 (also known as EpsinR; Hirst et al., 2004). Ii, in addition to interacting with AP1, can also interact with AP2, responsible for internalization from the plasma membrane (Kongsvik et al., 2002; Hofmann et al., 1999). Ii is essential for efficient trafficking of MHCII to the endosomal pathway and efficient antigen presentation, but can also deliver several other transmembrane proteins to endosomes, as discussed earlier. We now suggest that Vti1b, due to its interaction with Ii, is sorted to the early endosomal pathway in antigen-presenting cells and thus participates in controlling endosomal maturation and fusion.

Interestingly, Vti1b abundance in DCs was higher compared to that in HeLa cells and other non APCs tested in this work (Fig. S4A). Similarly, in the B16 melanoma cell line, Stx7 and Vamp8 SNAREs are upregulated as part of the specific machinery necessary for the biogenesis of melanosomes (Wade et al., 2001). A higher level of Vti1b protein in APCs could therefore be needed for specific transport steps fundamental for DC functions such as antigen processing and loading.

Here, we show that both the fusogenic properties of Ii and the maturation delay depend on Vti1b, because silencing Vti1b reversed the Ii-induced maturation delay in M1 and MelJuSo cells (Fig. 8). In this case, increased fusion mediated by Ii and the SNARE Vti1b, and possibly other interactors, on early endosomes would lead to a prolonged EE phase. Ii is also found to delay protein proteolysis (Gregers et al., 2003; Landsverk et al., 2011) and the part of the endosomal pathway that is trafficked by Ii would then create an ideal pathway for proteolytically processing instead of rapidly degrading

Journal of Cell Science (2020) 133, jcs244624. doi:10.1242/jcs.244624

antigenic proteins for MHC antigen loading of MHCI, MHCII and CD1, all of which associate with Ii.

Based on these data, we propose the following model. Ii binds directly or indirectly to Vti1b for transport via the PM to endosomes, where the complex can engage further in trans-SNARE complex formation. A higher degree of endosomal fusion dependent on a relocation of the 'late' SNARE Vti1b to early endosomes prolongs the EE phase and leads to a slower maturation, creating a less proteolytic endosomal pathway. The model further postulates that, because Ii-positive endosomal vesicles engage in homotypic fusion, then not only Ii but also associated molecules like MHCII can be concentrated in some late endosomal/lysosomal vesicles, described previously as the MIIC compartment (Peters et al., 1991).

It is very interesting that the expression of a single protein specific to antigen-presenting cells, Ii, has the ability to reshape the endosomal pathway in a specific way. Ii not only chaperones MHCII and other molecules to the loading compartment, but seems to be directly involved in shaping this specialized organelle of APCs. The antigen-loading compartment has a unique proteolytic environment, less aggressive than that of classical lysosomes (Neefjes, 1999), which is needed for efficient but not full processing of antigens. We suggest that this property is intricately connected to the ability of Ii to delay endosomal maturation. In addition, the antigen-loading compartments integrate antigen input from several sources other than endocytosis, such as phagocytosis, macropinocytosis and autophagy (Blum et al., 2013), but whether the transfer of these to the immunoendosome is by a general or a more specific mechanism is not known.

In conclusion, we show that the Qb SNARE Vti1b is involved in Ii-mediated endosomal fusion. Ii redistributes Vti1b from the Golgi to early endosomes, which leads to delayed maturation of endosomes. This mechanism of regulating the endosomal pathway could be critical for optimal MHCI and MHCII antigen loading and subsequent presentation, and thus for an efficient normal immune response.

MATERIALS AND METHODS

Cell lines

The human fibroblast-like M1 cells (Royer-Pokora et al., 1984), the M1 cells stably transfected with pMep4-Ii (Skjeldal et al., 2012), the human melanoma cell line MelJuSo (Johnson et al., 1981), the human lymphoblast cell line Raji (Pulvertaft, 1964), the human adenocarcinoma HeLa cells (ATCC CCL-2) and the rat neuronal Neuro2A cell line (a gift from Cecilia Bucci, University of Salento, Lecce, Italy; Cogli et al., 2013) were described previously. Healthy donor-derived Epstein-Barr virus growth-transformed lymphoblastoid cell lines (EBV-LCL) were provided by Sebastien Wälchli (Oslo University Hospital, Oslo, Norway).

Mononuclear cells were isolated from buffy coats from healthy donors through density-gradient centrifugation by using Lymphoprep® (Axis Shield, Dundee, UK). Buffy coats from anonymous donors were obtained from the local blood bank (Section for Immunology and Blood Transfusion, Ullevål University Hospital, Oslo, Norway) according to the guidelines of the local blood bank approved by the Norwegian Regional Committee for Medical Research Ethics. Monocyte-derived dendritic cells (MDDCs) were generated from plastic-adherent or directly isolated monocytes (Monocyte Isolation Kit II, Miltenyi Biotec, Bergisch Gladbach, Germany) through culture for 6 days in Roswell Park Memorial Institute medium (RPMI-1640; Lonza, Basel, Switzerland) containing 100 ng/ml granulocyte–macrophage colony stimulating factor (GM-CSF; Immunotools, Friesoythe, Germany) and 20 ng/ml IL-4 (Invitrogen, Life Technologies, Carlsbad, California, USA) supplemented with 10% fetal calf serum (FCS), 2 mM L-glutamine, 100 U/ml penicillin and 100 µg/ml streptomycin (Sigma, St Louis, Missouri, USA).

M1 and HeLa cell lines were grown in Dulbecco's Modified Eagle's Medium (DMEM; Lonza) supplemented with 10% FCS, 2 mM L-glutamine, 100 U/ml penicillin and 100 µg/ml streptomycin (all Sigma). Additionally, 200 µg/ml hygromycin B (Sigma) was added to stably transfected M1 cells. MelJuSo, Raji, EBV and MDDCs were grown in either Iscove's Modified Dulbecco's Medium (IMDM; for MelJuSo cells) or RPMI-1640 supplemented with 10% FCS, 2 mM L-glutamine, 100 U/ml penicillin and 100 µg/ml streptomycin. For live-cell microscopy, cells were grown in 35-mm glass-bottom dishes (MatTek, Ashland, Massachusetts, USA), 8-well glass-bottom µ-Slides (Ibidi, Grafelfing, Germany), or 4-chamber 35-mm glass-bottom dishes (CellVis, Mountain View, California, USA) for 24 h in complete medium.

Establishment of CRISPR/Cas9 Ii KO MelJuSo cell lines

The process of establishing CRISPR-Cas9 null alleles was described previous (Wijdeven et al., 2015). Briefly, MelJuSo cells were transfected with px330 Sp-Cas9 and sgRNA vectors (5′-TCGCGCTGGTCATCCATG-AC-3′ and 5′-GGAAGATCAGAAGCCAGTCA-3′ targeting Ii exon 1) together with a vector coding for blasticidin resistance using Lipofectamine® 2000. Successfully transfected cells were selected by treatment with blasticidin for 1 week. Colonies grown from resistant cells were picked, expanded and screened for Ii knockout by western blotting.

Constructs

mEGFP-C1 and mApple–Rab7 were from Addgene (plasmid numbers 54759 and 54945, respectively; deposited by Michael Davidson, Florida State University, Tallahassee, USA). His6–Ii p33 wt and His6–Δ27Ii in pCGFP-EU were purchased from GenScript. pCGFP-EU empty vector has been described before (Kawate and Gouaux, 2006) and was provided by Jens P. Morth (University of Oslo, Norway). mcherry–Rab5Q79L, mApple–Rab5, mcherry–Rab5, EGFP–Rab5Q79L and EGFP–Rab7 have been described previously (Bergeland et al., 2008; Stenmark et al., 1994; Bucci et al., 2000). The Vti1b–mCitrine plasmid was constructed as follows. The coding sequence of human *VTI1B* was amplified by PCR using 5′ and 3′ primers containing an EcoRI and a BamHI restriction site, respectively. Forward primer was 5′-AATCAGAATTCATGGCCTCCTCCG-3′; reverse primer was 5′-CATCGGATCCCAATGGCTGCGAAAGAATTTG-3′. The fragment was then subcloned into pECFP-N1 plasmid cut with EcoRI and BamHI. The identity of all plasmids was confirmed by Sanger sequencing (GATC biotech).

Antibodies and reagents

Primary antibodies: mouse anti-Ii (clone M-B741, targeting the extracellular/luminal domain, 555538; 1:500) and the anti-EEA1 antibody (BD610456; 1:100) were from BD Biosciences (Franklin Lakes, New Jersey, USA); mouse anti-tubulin (13-8000; 1:12,000) from Life Technologies (Carlsbad, California, USA); sheep anti-TGN46 (AHP500; 1:100) from AbD Serotec (Oxford, UK); rabbit anti-GFP (ab6556; 1:2000), rabbit anti-Vti1b (ab184170; 1:200 for western blotting), rabbit anti-giantin (ab24586; 1:1000), rabbit anti-CI-M6PR (ab32815; 1:200) from Abcam (Cambridge, UK). Alexa Fluor secondary antibodies (Invitrogen) were used at 1:200 dilution for immunofluorescence analyses. Secondary antibodies conjugated with horseradish peroxidase (GE Healthcare, Chicago, Illinois, USA) were used at 1:5000 for immunoblotting.

Anti-Ii for live immunostaining was labelled using a monoclonal antibody labelling kit (Molecular Probes, Eugene, Oregon, USA), according to the manufacturer's protocol, with Alexa Fluor-488, -555, or -647.

DAPI (Sigma-Aldrich) was used at 0.1 µg/ml. LysoTracker Deep Red, used at a concentration of 50 nM, and dextran–Alexa Fluor 488 (10,000 MW), used at a concentration of 0.5 mg/ml, were purchased from ThermoFisher (Waltham, Massachusetts, USA).

Poly-L-lysine (PLL, 0.01% solution), wortmannin and N-ethylmaleimide (NEM) were all purchased from Sigma.

siRNA transfection

Individual siRNAs were transfected by forward transfection using Lipofectamine® RNAiMax reagent (ThermoFisher) according to the manufacturer's protocol. In brief, 250,000 cells/well were seeded in 6-well plates (VWR, Radnor, Pennsylvania, USA) in 1 ml antibiotic-free medium 24 h prior to transfection. Transfection mixes were prepared by

diluting 2.5 µl siRNA stock (80 µM) in 250 µl Opti-MEM (ThermoFisher) and 6 µl RNAiMax in 250 µl Opti-MEM followed by immediate mixing of both. The transfection mixture was then incubated at room temperature for 20 min before addition to the cells. 4 h after transfection, 1 ml of complete medium was added. Medium on the cells was replaced the next day. 48 h after transfections, cells were washed twice with pre-warmed PBS, trypsinized for 1 min, resuspended in 2 ml complete medium and split between 35-mm imaging dishes (MatTek) or 8-well slides (Ibidi) for imaging and 6-well plates for lysis and subsequent biochemical assays.

Plasmid transfection

For plasmid transfection, cells were transfected using Lipofectamine® 2000 (ThermoFisher) according to the manufacturer's protocol. In brief, cells were seeded the day before transfection. Before transfection, the medium was replaced with Opti-MEM. Transfection mixes were prepared with 1.5 µl Lipofectamine® 2000 (ThermoFisher) per 1 µg of plasmid DNA. The transfection mix was then added dropwise to the cells.

Immunofluorescence

For immunofluorescence, cells were grown on 10×10 mm number 1.5 high-precision coverslips (Marienfeld, Germany). Cells were washed twice with ice-cold PBS, fixed at room temperature for 15 min with 3% paraformaldehyde, quenched for 2 min with 50 mM NH_4Cl, washed again twice with PBS, permeabilized for 15 min with 0.25% saponin (Sigma) in PBS, incubated with primary antibody for 20 min, washed three times for 5 min each with 0.1% saponin in PBS, incubated with appropriate secondary antibody for 20 min in the dark, washed three times for 5 min each with 0.1% saponin in PBS, washed twice with PBS, and mounted with Mowiol on glass slides (Thermo Fisher).

Endocytic trafficking assay

Cells were grown for 24 h on 35-mm 4-chamber glass-bottom dishes (CellVis) in complete medium without Phenol Red. Dextran and LysoTracker Deep Red were added, and cells incubated for 5 min at 37°C before removal of the dyes. Cells were washed three times to remove traces of the dyes. Imaging of the samples started 5 min after the removal of the dextran. Cells were imaged every 5 min.

Confocal imaging

Live imaging of transfected cells and imaging of immunostained cells was performed on a Zeiss LSM880 microscope equipped with a Plan Apo 63×1.4 NA oil immersion objective. Live cells were imaged using Fast AiryScan mode with optimal sampling for super-resolution.

Image processing and analysis

Endosome size was quantified using ImageJ software (NIH, Bethesda, MD, USA). In brief, confocal 3D stacks were maximum projected and, in the case of EGFP–Rab5Q79L images, the cytoplasmic background was subtracted using rolling-ball background subtraction. The resulting images where then binarized using a manually adjusted threshold for each image. After that, the images were inverted, morphologically opened, and objects split by watershed processing and manual splitting where needed. Finally, the analyse particles function was used to measure all objects. The Feret's diameter was used as the measurement of object size, and objects larger than 3 µm were considered enlarged endosomes. Violin plots showing the distribution of endosomal size and number were created with RStudio software and the ggplot2 package (RStudio, Inc.). Dextran–LysoTracker Deep Red colocalization was quantified using the colocalization function in ZEN blue software (Zeiss). Weighted colocalization coefficient was used as a measure of the colocalization of dextran with LysoTracker DeepRed.

Immunoblotting

Cell lysates were subjected to SDS–PAGE followed by blotting onto PVDF membranes (Millipore, Burlington, Massachusetts, USA), and probed with each primary antibody diluted in 2% blotting-grade non-fat dry milk (Bio-Rad, Hercules, California). Next, membranes were incubated with secondary antibodies conjugated to HRP and subsequently with SuperSignal West Femto Maximum Sensitivity Substrate (ThermoFisher) before digital imaging (Kodak image station 4000R) or detection with Amersham ECL Prime Western Blotting Detection Reagent before exposure on Amersham Hyperfilm ECL (both GE Healthcare).

Statistical analysis

Unless indicated otherwise, columns and error bars represent the mean ±s.e.m. of at least three independent experiments. Treatments were compared to control using two-tailed Student's *t*-test, either paired or unpaired as appropriate (Microsoft Excel), or ANOVA followed by Tukey's post hoc test in the GraphPad Prism 4 software when comparing multiple samples within the same graph (control versus Ii-expressing cells; Ii-expressing cells versus Ii-expressing vti1b-depleted cells). Differences were considered statistically significant at $P<0.05$ (indicated by *), $P<0.01$ (**) and $P<0.001$ (***), respectively.

Co-immunoprecipitation

Co-immunoprecipitation experiments using GFP-trap (ChromoTek, Munich, Germany) were performed according to the manufacturer's protocol. In brief, 1×10^6–2×10^6 cells were seeded on 10-cm cell culture dishes and incubated for 24 h at 37°C, 5% CO_2. The cells were then transfected using Lipofectamine 2000, as described above. M1 pMep4-Ii cells were treated with 7 µM $CdCl_2$ overnight to induce expression of Ii. Cells were washed twice with ice-cold PBS and lysed in 200 µl lysis buffer [10 mM Tris-HCl pH 7.5, 100 mM NaCl, 1 mM EDTA, Complete protease inhibitors (Sigma), 1 mM PMSF (Sigma) and 0.5% NP-40 (Sigma)] for 30 min on ice. Lysates were cleared by centrifugation at 13,000 ***g*** for 10 min at 4°C, diluted with 300 µl lysis buffer and loaded on magnetic agarose anti-GFP beads (GFP-trap_MA, ChromoTek) for 1 h at 4°C. Beads were then washed three times. Proteins were eluted using 2× Laemmli sample buffer with freshly added dithiothreitol (200 mM, Sigma-Aldrich) for 10 min at 95°C.

Acknowledgements

We thank Sebastien Wälchli (University of Oslo) for providing the EBV cells and Cecilia Bucci (University of Salento) for providing the Neuro2A cells. We thank Michael Davidson (Florida State University) for providing the mEGFP-C1 plasmid through Addgene and Jens P. Morth (University of Oslo) for the pCGFP-EU empty vector. We thank Frode M. Skjeldal (University of Oslo) and assistance with confocal imaging analysis and Xian Hu for assistance with manuscript writing and both for fruitful discussions. We thank Marita Borg Distefano for excellent technical assistance to improve western blots. Finally, we acknowledge the use of the NorMIC Oslo EuBI imaging node, Department of Biosciences, University of Oslo.

Competing interests

The authors declare no competing or financial interests.

Author contributions

Conceptualization: D.M.F., A.M, O.B.; Methodology: A.M., D.M.F., O.B., L.J., J.N.; Validation: A.M., D.F.; Formal analysis: A.M., D.M.F.; Investigation: A.M., D.M.F., I.H.S.O.B.; Resources: J.N., O.B.; Writing - original draft: A.M., D.M.F., O.B.; Writing - review & editing: A.M., O.B.; Visualization: A.M., D.M.F.; Supervision: O.B.; Project administration: O.B.; Funding acquisition: O.B.

Funding

We gratefully acknowledge the support from the Norges Forskningsråd (grants 214183 and 230770 to O.B.) and the Kreftforeningen (grant 113472 to O.B.).

Supplementary information

Supplementary information available online at
https://jcs.biologists.org/lookup/doi/10.1242/jcs.244624.supplemental

References

Antonin, W., Holroyd, C., Fasshauer, D., Pabst, S., Von Mollard, G. F. and Jahn, R. (2000). A SNARE complex mediating fusion of late endosomes defines conserved properties of SNARE structure and function. *EMBO J.* **19**, 6453-6464. doi:10.1093/emboj/19.23.6453

Bakke, O. and Dobberstein, B. (1990). MHC class II-associated invariant chain contains a sorting signal for endosomal compartments. *Cell* **63**, 707-716. doi:10.1016/0092-8674(90)90137-4

Basha, G., Omilusik, K., Chavez-Steenbock, A., Reinicke, A. T., Lack, N., Choi, K. B. and Jefferies, W. A. (2012). A CD74-dependent MHC class I endolysosomal cross-presentation pathway. *Nat. Immunol.* **13**, 237-245. doi:10.1038/ni.2225

Bayer-Santos, E., Durkin, C. H., Rigano, L. A., Kupz, A., Alix, E., Cerny, O., Jennings, E., Liu, M., Ryan, A. S., Lapaque, N. et al. (2016). The Salmonella Effector SteD Mediates MARCH8-Dependent Ubiquitination of MHC II Molecules and Inhibits T Cell Activation. *Cell Host Microbe* **20**, 584-595. doi:10.1016/j.chom.2016.10.007

Bergeland, T., Haugen, L., Landsverk, O. J., Stenmark, H. and Bakke, O. (2008). Cell-cycle-dependent binding kinetics for the early endosomal tethering factor EEA1. *EMBO Rep.* **9**, 171-178. doi:10.1038/sj.embor.7401152

Bikoff, E. K., Huang, L. Y., Episkopou, V., Van Meerwijk, J., Germain, R. N. and Robertson, E. J. (1993). Defective major histocompatibility complex class II assembly, transport, peptide acquisition, and CD4+ T cell selection in mice lacking invariant chain expression. *J. Exp. Med.* **177**, 1699-1712. doi:10.1084/jem.177.6.1699

Blum, J. S., Wearsch, P. A. and Cresswell, P. (2013). Pathways of antigen processing. *Annu. Rev. Immunol.* **31**, 443-473. doi:10.1146/annurev-immunol-032712-095910

Brachet, V., Pehau-Arnaudet, G., Desaymard, C., Raposo, G. and Amigorena, S. (1999). Early endosomes are required for major histocompatiblity complex class II transport to peptide-loading compartments. *Mol. Biol. Cell* **10**, 2891-2904. doi:10.1091/mbc.10.9.2891

Bremnes, B., Madsen, T., Gedde-Dahl, M. and Bakke, O. (1994). An LI and ML motif in the cytoplasmic tail of the MHC-associated invariant chain mediate rapid internalization. *J. Cell Sci.* **107**, 2021-2032.

Brunger, A. T. (2005). Structure and function of SNARE and SNARE-interacting proteins. *Q. Rev. Biophys.* **38**, 1-47. doi:10.1017/S0033583505004051

Bucci, C., Thomsen, P., Nicoziani, P., McCarthy, J. and Van Deurs, B. (2000). Rab7: a key to lysosome biogenesis. *Mol. Biol. Cell* **11**, 467-480. doi:10.1091/mbc.11.2.467

Caplan, S., Dell'angelica, E. C., Gahl, W. A. and Bonifacino, J. S. (2000). Trafficking of major histocompatibility complex class II molecules in human B-lymphoblasts deficient in the AP-3 adaptor complex. *Immunol. Lett.* **72**, 113-117. doi:10.1016/S0165-2478(00)00176-0

Cogli, L., Progida, C., Thomas, C. L., Spencer-Dene, B., Donno, C., Schiavo, G. and Bucci, C. (2013). Charcot-Marie-Tooth type 2B disease-causing RAB7A mutant proteins show altered interaction with the neuronal intermediate filament peripherin. *Acta Neuropathol.* **125**, 257-272. doi:10.1007/s00401-012-1063-8

Cuenda, A., Rouse, J., Doza, Y. N., Meier, R., Cohen, P., Gallagher, T. F., Young, P. R. and Lee, J. C. (1995). SB 203580 is a specific inhibitor of a MAP kinase homologue which is stimulated by cellular stresses and interleukin-1. *FEBS Lett.* **364**, 229-233. doi:10.1016/0014-5793(95)00357-F

Dressel, R., Elsner, L., Novota, P., Kanwar, N. and Fischer Von Mollard, G. (2010). The exocytosis of lytic granules is impaired in Vti1b- or Vamp8-deficient CTL leading to a reduced cytotoxic activity following antigen-specific activation. *J. Immunol.* **185**, 1005-1014. doi:10.4049/jimmunol.1000770

Dugast, M., Toussaint, H., Dousset, C. and Benaroch, P. (2005). AP2 clathrin adaptor complex, but not AP1, controls the access of the major histocompatibility complex (MHC) class II to endosomes. *J. Biol. Chem.* **280**, 19656-19664. doi:10.1074/jbc.M501357200

Elliott, E. A., Drake, J. R., Amigorena, S., Elsemore, J., Webster, P., Mellman, I. and Flavell, R. A. (1994). The invariant chain is required for intracellular transport and function of major histocompatibility complex class II molecules. *J. Exp. Med.* **179**, 681-694. doi:10.1084/jem.179.2.681

Fasshauer, D., Sutton, R. B., Brunger, A. T. and Jahn, R. (1998). Conserved structural features of the synaptic fusion complex: SNARE proteins reclassified as Q- and R-SNAREs. *Proc. Natl Acad. Sci. USA* **95**, 15781-15786. doi:10.1073/pnas.95.26.15781

Fischer Von Mollard, G. and Stevens, T. H. (1999). The Saccharomyces cerevisiae v-SNARE Vti1p is required for multiple membrane transport pathways to the vacuole. *Mol. Biol. Cell* **10**, 1719-1732. doi:10.1091/mbc.10.6.1719

Furuta, N., Fujita, N., Noda, T., Yoshimori, T. and Amano, A. (2010). Combinational soluble N-ethylmaleimide-sensitive factor attachment protein receptor proteins VAMP8 and Vti1b mediate fusion of antimicrobial and canonical autophagosomes with lysosomes. *Mol. Biol. Cell* **21**, 1001-1010. doi:10.1091/mbc.e09-08-0693

Gorvel, J.-P., Escola, J.-M., Stang, E. and Bakke, O. (1995). Invariant chain induces a delayed transport from early to late endosomes. *J. Biol. Chem.* **270**, 2741-2746. doi:10.1074/jbc.270.6.2741

Gregers, T. F., Nordeng, T. W., Birkeland, H. C., Sandlie, I. and Bakke, O. (2003). The cytoplasmic tail of invariant chain modulates antigen processing and presentation. *Eur. J. Immunol.* **33**, 277-286. doi:10.1002/immu.200310001

Haugen, L. H., Skjeldal, F. M., Bergeland, T. and Bakke, O. (2017). Endosomal binding kinetics of Eps15 and Hrs specifically regulate the degradation of RTKs. *Sci. Rep.* **7**, 17962. doi:10.1038/s41598-017-17320-2

Hille-Rehfeld, A. (1995). Mannose 6-phosphate receptors in sorting and transport of lysosomal enzymes. *Biochim. Biophys. Acta* **1241**, 177-194. doi:10.1016/0304-4157(95)00004-B

Hirst, J., Miller, S. E., Taylor, M. J., Von Mollard, G. F. and Robinson, M. S. (2004). EpsinR is an adaptor for the SNARE protein Vti1b. *Mol. Biol. Cell* **15**, 5593-5602. doi:10.1091/mbc.e04-06-0468

Hofmann, M. W., Höning, S., Rodionov, D., Dobberstein, B., Von Figura, K. and Bakke, O. (1999). The leucine-based sorting motifs in the cytoplasmic domain of the invariant chain are recognized by the clathrin adaptors AP1 and AP2 and their medium chains. *J. Biol. Chem.* **274**, 36153-36158. doi:10.1074/jbc.274.51.36153

Jahn, R. and Scheller, R. H. (2006). SNAREs – engines for membrane fusion. *Nat. Rev. Mol. Cell Biol.* **7**, 631-643. doi:10.1038/nrm2002

Johnson, J. P., Demmer-Dieckmann, M., Meo, T., Hadam, M. R. and Riethmuller, G. (1981). Surface antigens of human melanoma cells defined by monoclonal antibodies. I. Biochemical characterization of two antigens found on cell lines and fresh tumors of diverse tissue origin. *Eur. J. Immunol.* **11**, 825-831.

Jones, A. T. and Clague, M. J. (1995). Phosphatidylinositol 3-kinase activity is required for early endosome fusion. *Biochem. J.* **311**, 31-34. doi:10.1042/bj3110031

Kampgen, E., Koch, N., Koch, F., Stoger, P., Heufler, C., Schuler, G. and Romani, N. (1991). Class II major histocompatibility complex molecules of murine dendritic cells: synthesis, sialylation of invariant chain, and antigen processing capacity are down-regulated upon culture. *Proc. Natl Acad. Sci. USA* **88**, 3014-3018. doi:10.1073/pnas.88.8.3014

Kawate, T. and Gouaux, E. (2006). Fluorescence-detection size-exclusion chromatography for precrystallization screening of integral membrane proteins. *Structure* **14**, 673-681. doi:10.1016/j.str.2006.01.013

Koch, N., Lipp, J., Pessara, U., Schenck, K., Wraight, C. and Dobberstein, B. (1989). MHC class II invariant chains in antigen processing and presentation. *Trends Biochem. Sci.* **14**, 383-386. doi:10.1016/0968-0004(89)90013-3

Kongsvik, T. L., Honing, S., Bakke, O. and Rodionov, D. G. (2002). Mechanism of interaction between leucine-based sorting signals from the invariant chain and clathrin-associated adaptor protein complexes AP1 and AP2. *J. Biol. Chem.* **277**, 16484-16488. doi:10.1074/jbc.M201583200

Kreykenbohm, V., Wenzel, D., Antonin, W., Atlachkine, V. and Von Mollard, G. F. (2002). The SNAREs vti1a and vti1b have distinct localization and SNARE complex partners. *Eur. J. Cell Biol.* **81**, 273-280. doi:10.1078/0171-9335-00247

Landsverk, O. J., Bakke, O. and Gregers, T. F. (2009). MHC II and the endocytic pathway: regulation by invariant chain. *Scand. J. Immunol.* **70**, 184-193. doi:10.1111/j.1365-3083.2009.02301.x

Landsverk, O. J., Barois, N., Gregers, T. F. and Bakke, O. (2011). Invariant chain increases the half-life of MHC II by delaying endosomal maturation. *Immunol. Cell Biol.* **89**, 619-629. doi:10.1038/icb.2010.143

Landsverk, O. J., Ottesen, A. H., Berg-Larsen, A., Appel, S. and Bakke, O. (2012). Differential regulation of MHC II and invariant chain expression during maturation of monocyte-derived dendritic cells. *J. Leukoc. Biol.* **91**, 729-737. doi:10.1189/jlb.0311150

Lesteberg, K., Orange, J. and Makedonas, G. (2017). Recycling endosomes in human cytotoxic T lymphocytes constitute an auxiliary intracellular trafficking pathway for newly synthesized perforin. *Immunol. Res.* **65**, 1031-1045. doi:10.1007/s12026-017-8945-8

Linstedt, A. D. and Hauri, H. P. (1993). Giantin, a novel conserved Golgi membrane protein containing a cytoplasmic domain of at least 350 kDa. *Mol. Biol. Cell* **4**, 679-693. doi:10.1091/mbc.4.7.679

Liu, S.-H., Marks, M. S. and Brodsky, F. M. (1998). A dominant-negative clathrin mutant differentially affects trafficking of molecules with distinct sorting motifs in the class II major histocompatibility complex (MHC) pathway. *J. Cell Biol.* **140**, 1023-1037. doi:10.1083/jcb.140.5.1023

Long, E. O., Lavaute, T., Pinet, V. and Jaraquemada, D. (1994). Invariant chain prevents the HLA-DR-restricted presentation of a cytosolic peptide. *J. Immunol.* **153**, 1487-1494.

Luzio, J. P., Parkinson, M. D., Gray, S. R. and Bright, N. A. (2009). The delivery of endocytosed cargo to lysosomes. *Biochem. Soc. Trans.* **37**, 1019-1021. doi:10.1042/BST0371019

Machamer, C. E. and Cresswell, P. (1982). Biosynthesis and glycosylation of the invariant chain associated with HLA-DR antigens. *J. Immunol.* **129**, 2564-2569.

Manderson, A. P., Kay, J. G., Hammond, L. A., Brown, D. L. and Stow, J. L. (2007). Subcompartments of the macrophage recycling endosome direct the differential secretion of IL-6 and TNFα. *J. Cell Biol.* **178**, 57-69. doi:10.1083/jcb.200612131

McCormick, P. J., Martina, J. A. and Bonifacino, J. S. (2005). Involvement of clathrin and AP-2 in the trafficking of MHC class II molecules to antigen-processing compartments. *Proc. Natl Acad. Sci. USA* **102**, 7910-7915. doi:10.1073/pnas.0502206102

Motta, A., Amodeo, P., Fucile, P., Morelli, M. A. C., Bremnes, B. and Bakke, O. (1997). A new triple-stranded α-helical bundle in solution: the assembling of the cytosolic tail of MHC-associated invariant chain. *Structure* **5**, 1453-1464. doi:10.1016/S0969-2126(97)00295-5

Murray, R. Z., Wylie, F. G., Khromykh, T., Hume, D. A. and Stow, J. L. (2005). Syntaxin 6 and Vti1b form a novel SNARE complex, which is up-regulated in activated macrophages to facilitate exocytosis of tumor necrosis Factor-α. *J. Biol. Chem.* **280**, 10478-10483. doi:10.1074/jbc.M414420200

Neefjes, J. (1999). CIIV, MIIC and other compartments for MHC class II loading. *Eur. J. Immunol.* **29**, 1421-1425. doi:10.1002/(SICI)1521-4141(199905)29:05<1421::AID-IMMU1421>3.0.CO;2-C

Neefjes, J. J. and Ploegh, H. L. (1992). Inhibition of endosomal proteolytic activity by leupeptin blocks surface expression of MHC class II molecules and their conversion to SDS resistance alpha beta heterodimers in endosomes. *EMBO J.* **11**, 411-416. doi:10.1002/j.1460-2075.1992.tb05069.x

Neefjes, J., Jongsma, M. L. M., Paul, P. and Bakke, O. (2011). Towards a systems understanding of MHC class I and MHC class II antigen presentation. *Nat. Rev. Immunol.* **11**, 823-836. doi:10.1038/nri3084

Nordeng, T. W., Gregers, T. F., Kongsvik, T. L., Méresse, S., Gorvel, J.-P., Jourdan, F., Motta, A. and Bakke, O. (2002). The cytoplasmic tail of invariant chain regulates endosome fusion and morphology. *Mol. Biol. Cell* **13**, 1846-1856. doi:10.1091/mbc.01-10-0478

Nozawa, T., Minowa-Nozawa, A., Aikawa, C. and Nakagawa, I. (2017). The STX6-VTI1B-VAMP3 complex facilitates xenophagy by regulating the fusion between recycling endosomes and autophagosomes. *Autophagy* **13**, 57-69. doi:10.1080/15548627.2016.1241924

Offenhauser, C., Lei, N., Roy, S., Collins, B. M., Stow, J. L. and Murray, R. Z. (2011). Syntaxin 11 binds Vti1b and regulates late endosome to lysosome fusion in macrophages. *Traffic* **12**, 762-773. doi:10.1111/j.1600-0854.2011.01189.x

Paul, P., Van Den Hoorn, T., Jongsma, M. L., Bakker, M. J., Hengeveld, R., Janssen, L., Cresswell, P., Egan, D. A., Van Ham, M., Ten Brinke, A. et al. (2011). A Genome-wide Multidimensional RNAi Screen Reveals Pathways Controlling MHC Class II Antigen Presentation. *Cell* **145**, 268-283. doi:10.1016/j.cell.2011.03.023

Peters, P. J., Neefjes, J. J., Oorschot, V., Ploegh, H. L. and Geuze, H. J. (1991). Segregation of MHC class II molecules from MHC class I molecules in the Golgi complex for transport to lysosomal compartments. *Nature* **349**, 669-676. doi:10.1038/349669a0

Pieters, J., Horstmann, H., Bakke, O., Griffiths, G. and Lipp, J. (1991). Intracellular transport and localization of major histocompatibility complex class II molecules and associated invariant chain. *J. Cell Biol.* **115**, 1213-1223. doi:10.1083/jcb.115.5.1213

Pieters, J., Bakke, O. and Dobberstein, B. (1993). The MHC class II-associated invariant chain contains two endosomal targeting signals within its cytoplasmic tail. *J. Cell Sci.* **106**, 831-846.

Powis, G., Bonjouklian, R., Berggren, M. M., Gallegos, A., Abraham, R., Ashendel, C., Zalkow, L., Matter, W. F., Dodge, J., Grindey, G. et al. (1994). Wortmannin, a potent and selective inhibitor of phosphatidylinositol-3-kinase. *Cancer Res.* **54**, 2419-2423.

Prescott, A. R., Lucocq, J. M., James, J., Lister, J. M. and Ponnambalam, S. (1997). Distinct compartmentalization of TGN46 and beta 1,4-galactosyltransferase in HeLa cells. *Eur. J. Cell Biol.* **72**, 238-246.

Pryor, P. R., Mullock, B. M., Bright, N. A., Lindsay, M. R., Gray, S. R., Richardson, S. C., Stewart, A., James, D. E., Piper, R. C. and Luzio, J. P. (2004). Combinatorial SNARE complexes with VAMP7 or VAMP8 define different late endocytic fusion events. *EMBO Rep.* **5**, 590-595. doi:10.1038/sj.embor.7400150

Pulvertaft, J. V. (1964). Cytology of Burkitt's Tumour (African Lymphoma). *Lancet* **283**, 238-240. doi:10.1016/S0140-6736(64)92345-1

Qu, B., Pattu, V., Junker, C., Schwarz, E. C., Bhat, S. S., Kummerow, C., Marshall, M., Matti, U., Neumann, F., Pfreundschuh, M. et al. (2011). Docking of lytic granules at the immunological synapse in human CTL requires Vti1b-dependent pairing with CD3 endosomes. *J. Immunol.* **186**, 6894-6904. doi:10.4049/jimmunol.1003471

Roche, P. A., Teletski, C. L., Stang, E., Bakke, O. and Long, E. O. (1993). Cell surface HLA-DR-invariant chain complexes are targeted to endosomes by rapid internalization. *Proc. Natl Acad. Sci. USA* **90**, 8581-8585. doi:10.1073/pnas.90.18.8581

Romagnoli, P., Layet, C., Yewdell, J., Bakke, O. and Germain, R. N. (1993). Relationship between invariant chain expression and major histocompatibility complex class II transport into early and late endocytic compartments. *J. Exp. Med.* **177**, 583-596. doi:10.1084/jem.177.3.583

Royer-Pokora, B., Peterson, Jr., W. D. and Haseltine, W. A. (1984). Biological and biochemical characterization of an SV40-transformed xeroderma pigmentosum cell line. *Exp. Cell Res.* **151**, 408-420. doi:10.1016/0014-4827(84)90391-4

Sand, K. M., Landsverk, O. J., Berg-Larsen, A., Bakke, O. and Gregers, T. F. (2014). The human-specific invariant chain isoform Iip35 modulates Iip33 trafficking and function. *Immunol. Cell Biol.* **92**, 791-798. doi:10.1038/icb.2014.54

Schröder, B. (2016). The multifaceted roles of the invariant chain CD74 – More than just a chaperone. *Biochim. Biophys. Acta.* **1863**, 1269-1281. doi:10.1016/j.bbamcr.2016.03.026

Sevilla, L. M., Richter, S. S. and Miller, J. (2001). Intracellular transport of MHC class II and associated invariant chain in antigen presenting cells from AP-3-deficient mocha mice. *Cell. Immunol.* **210**, 143-153. doi:10.1006/cimm.2001.1817

Skjeldal, F. M., Strunze, S., Bergeland, T., Walseng, E., Gregers, T. F. and Bakke, O. (2012). The fusion of early endosomes induces molecular-motor-driven tubule formation and fission. *J. Cell Sci.* **125**, 1910-1919. doi:10.1242/jcs.092569

Stang, E. and Bakke, O. (1997). MHC class II-associated invariant chain-induced enlarged endosomal structures: a morphological study. *Exp. Cell Res.* **235**, 79-92. doi:10.1006/excr.1997.3617

Stenmark, H., Parton, R. G., Steele-Mortimer, O., Lütcke, A., Gruenberg, J. and Zerial, M. (1994). Inhibition of rab5 GTPase activity stimulates membrane fusion in endocytosis. *EMBO J.* **13**, 1287-1296. doi:10.1002/j.1460-2075.1994.tb06381.x

Von Mollard, G. F., Nothwehr, S. F. and Stevens, T. H. (1997). The yeast v-SNARE Vti1p mediates two vesicle transport pathways through interactions with the t-SNAREs Sed5p and Pep12p. *J. Cell Biol.* **137**, 1511-1524. doi:10.1083/jcb.137.7.1511

Wade, N., Bryant, N. J., Connolly, L. M., Simpson, R. J., Luzio, J. P., Piper, R. C. and James, D. E. (2001). Syntaxin 7 complexes with mouse Vps10p tail interactor 1b, syntaxin 6, vesicle-associated membrane protein (VAMP)8, and VAMP7 in b16 melanoma cells. *J. Biol. Chem.* **276**, 19820-19827. doi:10.1074/jbc.M010838200

Walchli, S., Kumari, S., Fallang, L.-E., Sand, K. M., Yang, W., Landsverk, O. J., Bakke, O., Olweus, J. and Gregers, T. F. (2014). Invariant chain as a vehicle to load antigenic peptides on human MHC class I for cytotoxic T-cell activation. *Eur. J. Immunol.* **44**, 774-784. doi:10.1002/eji.201343671

Wang, K., Peterson, P. A. and Karlsson, L. (1997). Decreased endosomal delivery of major histocompatibility complex class II-invariant chain complexes in dynamin-deficient cells. *J. Biol. Chem.* **272**, 17055-17060. doi:10.1074/jbc.272.27.17055

Wegner, C. S., Malerod, L., Pedersen, N. M., Progida, C., Bakke, O., Stenmark, H. and Brech, A. (2010). Ultrastructural characterization of giant endosomes induced by GTPase-deficient Rab5. *Histochem. Cell Biol.* **133**, 41-55. doi:10.1007/s00418-009-0643-8

Weimbs, T., Low, S. H., Chapin, S. J., Mostov, K. E., Bucher, P. and Hofmann, K. (1997). A conserved domain is present in different families of vesicular fusion proteins: a new superfamily. *Proc. Natl Acad. Sci. USA* **94**, 3046-3051. doi:10.1073/pnas.94.7.3046

Wymann, M. P., Bulgarelli-Leva, G., Zvelebil, M. J., Pirola, L., Vanhaesebroeck, B., Waterfield, M. D. and Panayotou, G. (1996). Wortmannin inactivates phosphoinositide 3-kinase by covalent modification of Lys-802, a residue involved in the phosphate transfer reaction. *Mol. Cell. Biol.* **16**, 1722-1733. doi:10.1128/MCB.16.4.1722

Wijdeven, R. H., Pang, B., van der Zanden, S. Y., Qiao, X., Blomen, V., Hoogstraat, M., Lips, E. H., Janssen, L., Wessels, L., Brummelkamp, T. R. et al. (2015). Genome-wide identification and characterization of novel factors conferring Resistance to topoisomerase II poisons in cancer. Cancer Res. **75**, 4176-4187. doi:10.1158/0008-5472.CAN-15-0380

Ye, L., Liu, X., Rout, S. N., Li, Z., Yan, Y., Lu, L., Kamala, T., Nanda, N. K., Song, W., Samal, S. K. et al. (2008). The MHC class II-associated invariant chain interacts with the neonatal Fc gamma receptor and modulates its trafficking to endosomal/lysosomal compartments. *J. Immunol.* **181**, 2572-2585. doi:10.4049/jimmunol.181.4.2572

Supplementary information

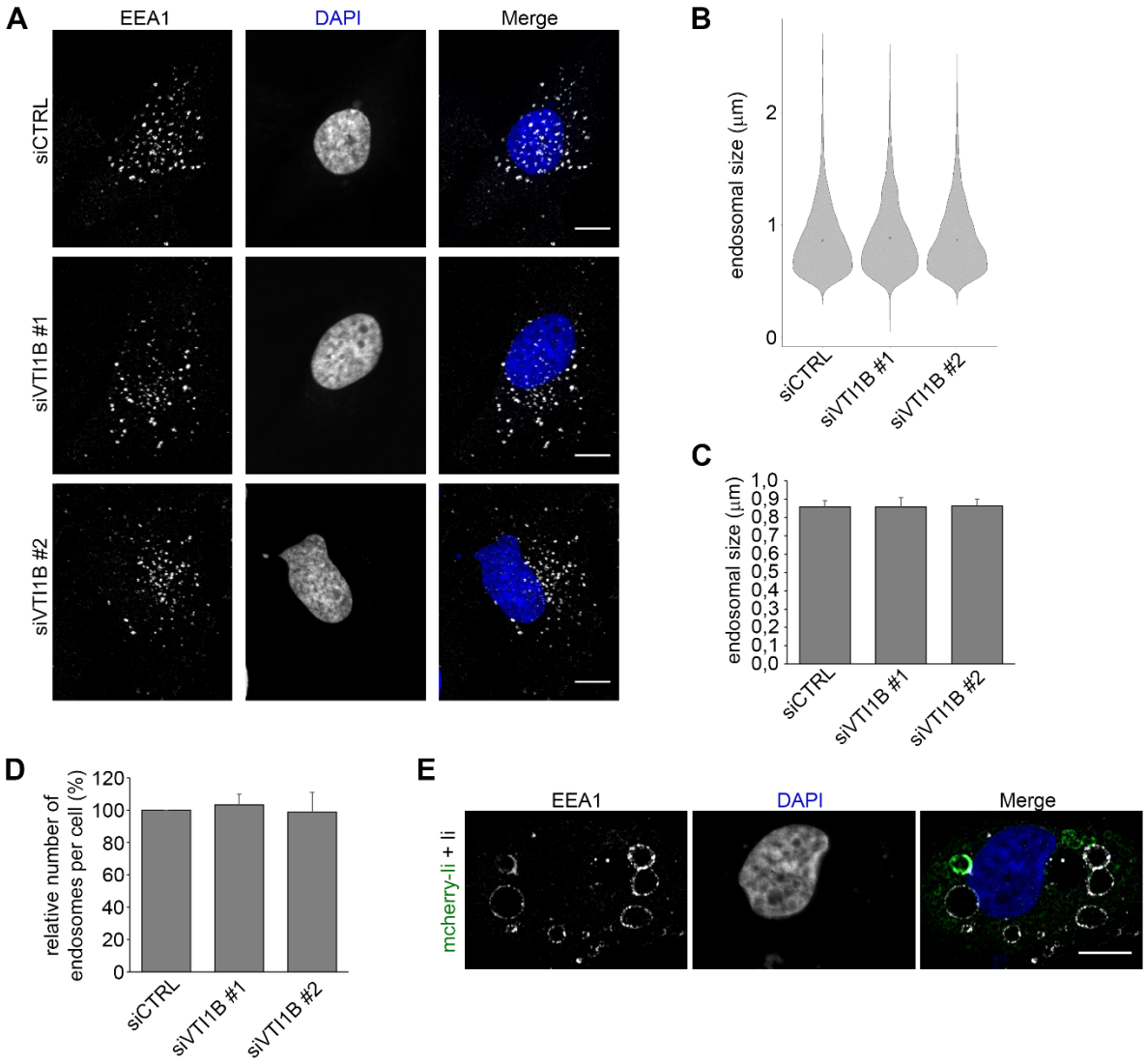

Figure S1

Figure S1. Size of early endosomes is not altered in M1 cells depleted of Vti1b compared to control cells. A) M1 cells (not expressing Ii) have been treated with control siRNA (siCTRL) or siRNAs against VTI1B (siVTI1B #1 or siVTI1B #2). Subsequently, cells have been fixed and stained with α-EEA1 antibody and DAPI. Maximum projections are shown (Scale bars: 10 µm B). Violin plot showing the distribution of the size of endosomes positive for EEA1 in control and VTI1B-depleted cells. Size of at least 2500 endosomes per sample have been analysed. C) Quantification of the average endosomal size in control or VTI1B-depleted cells. Data represent the mean ± s.e.m. of three independent experiments. At least 48 cells per condition have been analysed. D) Quantification of the number of endosomes in control cells and in cells silenced for VTI1B. Data represent the mean ± s.e.m. of three independent experiments. At least 48 cells per condition have been analysed. E) M1 cell transfected with mcherry-Ii and untagged-Ii and stained with α-EEA1 antibody and DAPI is shown. Enlarged EEA1-positive endosomes are shown. Scale bar: 10 µm.

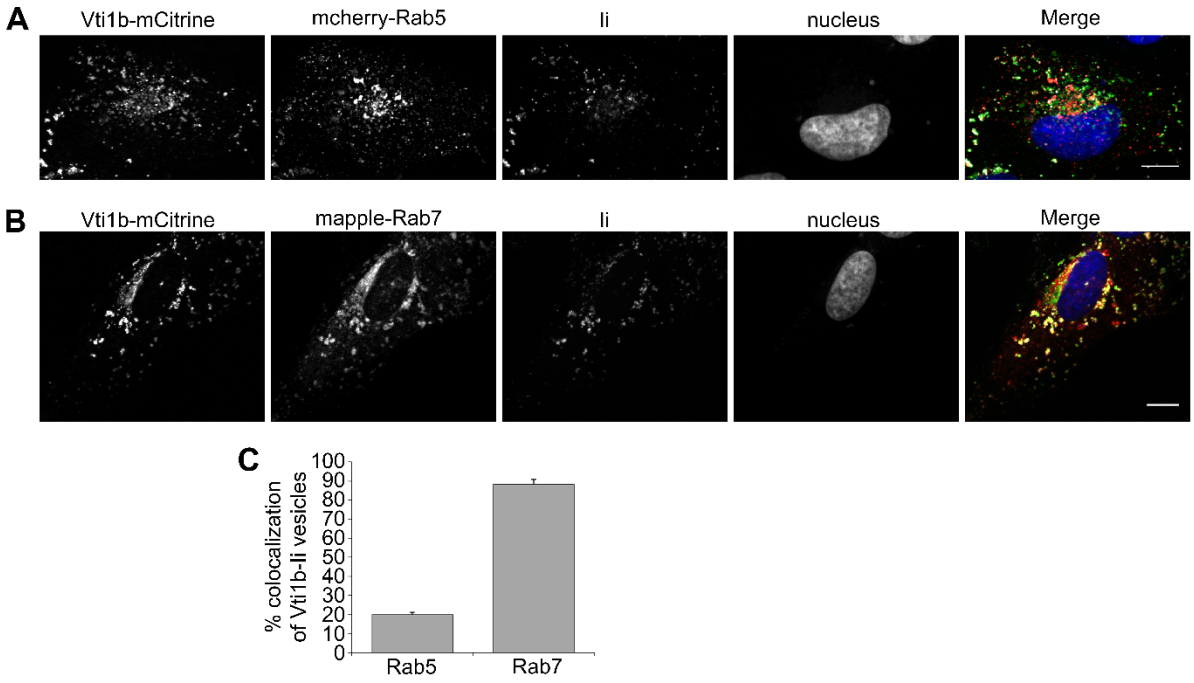

Figure S2

Figure S2. Vti1b and Ii colocalize together on Rab5- or Rab7-positive endosomes. A) MelJuSo control cells have been transfected with Vti1b-mCitrine (green) and mcherry-Rab5 (red) and subsequently fixed and stained for Ii and nuclei. Maximal projections are shown. Scale bar: 10 µm. B) MelJuSo control cells have been transfected with Vti1b-mCitrine (green) and mapple-Rab7 (red) and subsequently fixed and stained for Ii and nuclei. Scale bar: 10 µm. Maximal projections are shown. C) Percentage of colocalization of Vti1b and Ii on Rab5-positive vesicles or Rab7-positive vesicles is indicated. Experiments have been performed in triplicate. Averages ± s.e.m. are indicated. Number of endosomes analysed was 411 per mcherry-Rab5 transfected cells and 767 for mapple-Rab7 transfected cells.

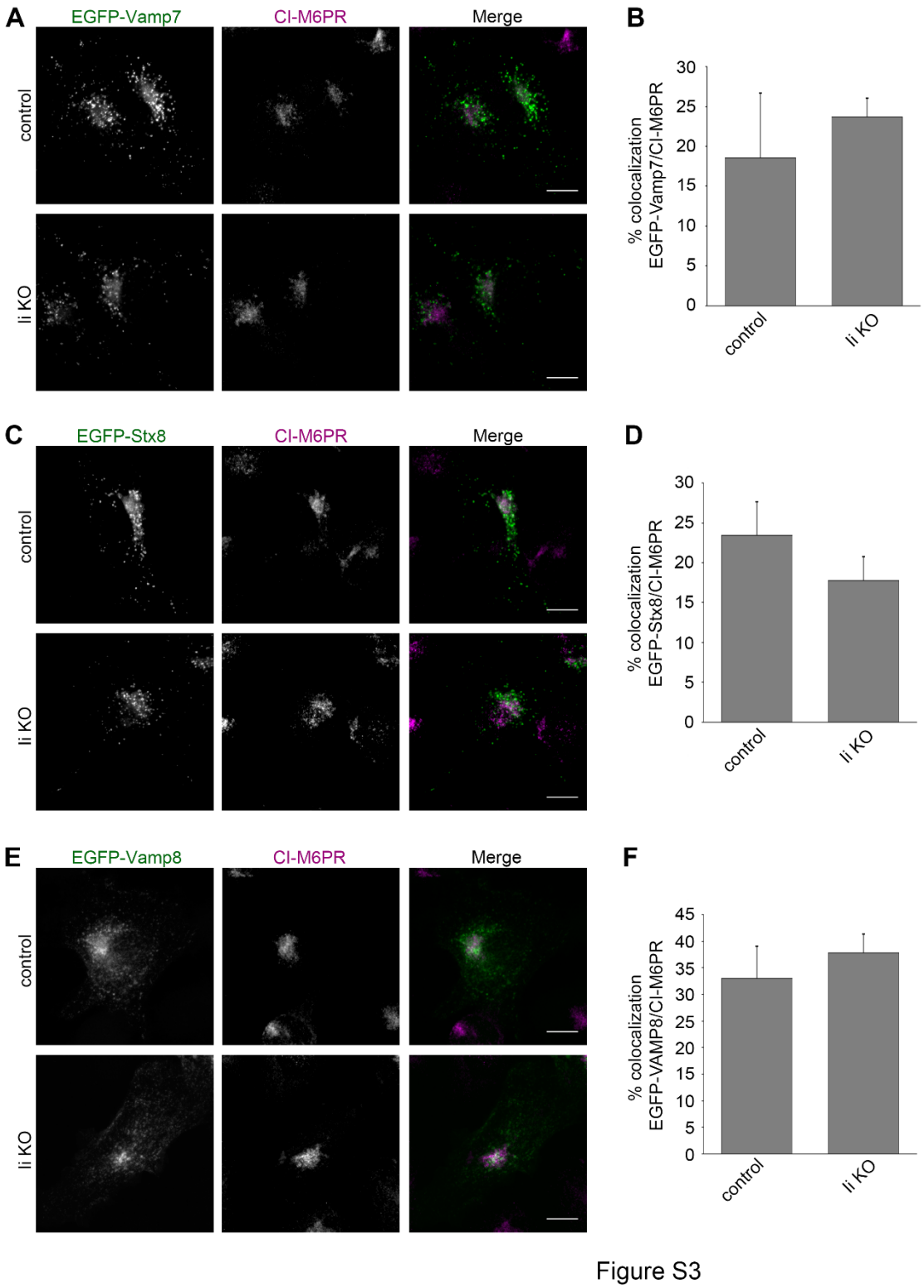

Figure S3

Figure S3. Localization of Vamp7, Stx8 and Vamp8 is not altered in MelJuSo Ii KO cells. A) MelJuSo control and Ii KO cells have been transfected with EGFP-Vamp7 and subsequently stained after fixation with an anti-CI-M6PR antibody. Representative images (maximal projections) of EGFP-Vamp7 (green) and CI-M6PR (magenta) and merge are shown. Scale bars: 10 µm. B) Quantification of the percentage of colocalization between

EGFP-Vamp7 and CI-M6PR in control and Ii KO cells is shown. C) MelJuSo control and Ii KO cells have been transfected with EGFP-Stx8 and subsequently stained after fixation with an anti-CI-M6PR antibody. Representative images (maximal projections) of EGFP-Stx8 (green) and CI-M6PR (magenta) and merge are shown. Scale bars: 10 µm. D) Quantification of the percentage of colocalization between EGFP-Stx8 and CI-M6PR in control and Ii KO cells is shown. E) MelJuSo control and Ii KO cells have been transfected with EGFP-Vamp8 and subsequently stained after fixation with an anti-CI-M6PR antibody. Representative images (maximal projections) of EGFP-Vamp8 (green) and CI-M6PR (magenta) and merge are shown. Scale bars: 10 µm. D) Quantification of the percentage of colocalization between EGFP-Vamp8 and CI-M6PR in control and Ii KO cells is shown.

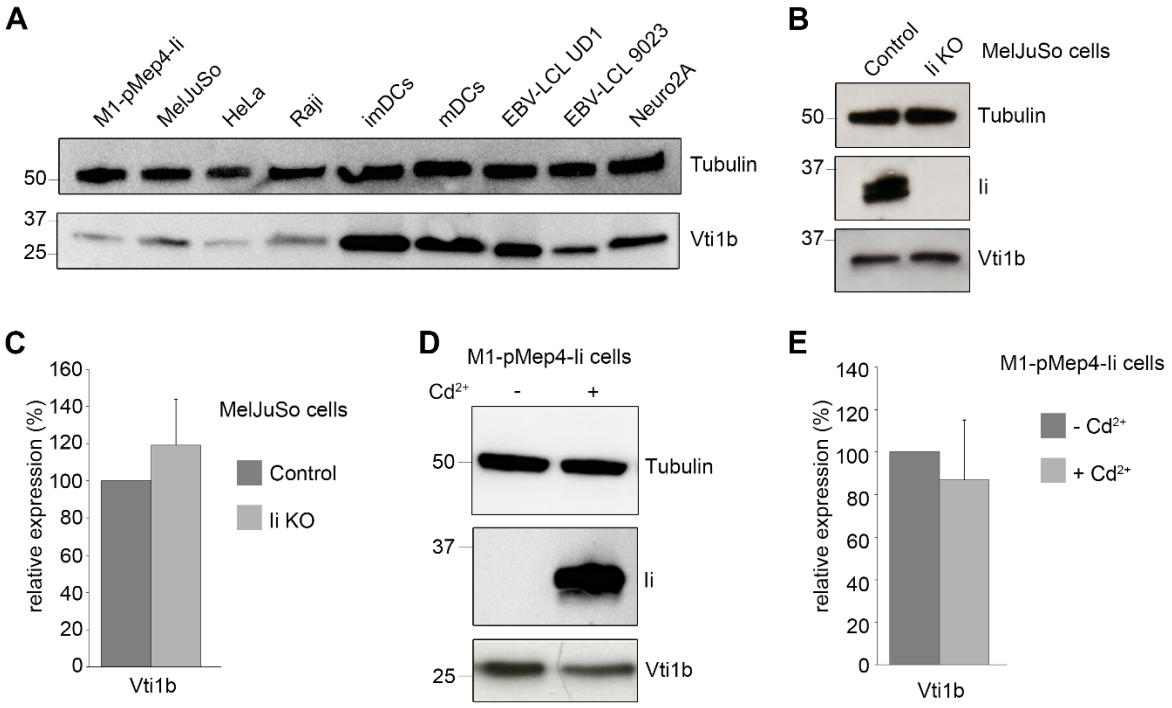

Figure S4

Fig. S4. Expression levels of candidate proteins in different cell types. A) Lysates of several cell types as indicated in the figure have been subjected to western blot analysis using anti-Vti1b and anti-tubulin antibodies. B) MelJuSo control and Ii KO cells have been lysed and relative samples have been subjected to western blot analysis. Antibodies against Vti1b, Ii and tubulin have been used. C) Quantification of Vti1b abundance in MelJuSo control and Ii KO cells. Data represent the mean ± s.e.m. of three independent experiments. D) Control M1-pMep4-Ii wt cells not expressing Ii ($-Cd^{2+}$) or after treatment with 7µM $CdCl_2$ overnight to induce the expression of Ii ($+Cd^{2+}$) have been lysed. Lysates were subjected to western blot analysis using anti-Vti1b, anti-Ii and anti-tubulin antibodies. E) Quantification of Vti1b abundance in M1-pMep4-Ii wt cells expressing ($+Cd^{2+}$) or not ($-Cd^{2+}$) Ii is shown. Data represent the mean ± s.e.m. of three independent experiments.

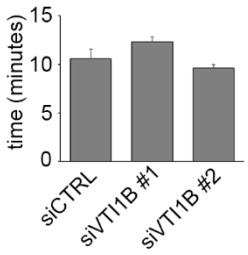

Figure S5

Fig. S5. Vti1b depletion does not affect endosomal maturation in absence of Ii. Quantification of the time until the Rab5-Rab7 switch is shown. Mean ± s.e.m. for at least three independent experiments. 65 endosomes were analysed for control siRNA, 30 for Vti1b siRNA #1, and 53 for Vti1b siRNA #2 cells) from several cells. The measurements of each individual endosome depend on its visibility in time and space and, therefore, are not precisely accurate.